



Norwegian University of
Science and Technology

Study of Piezoelectric and Mechanical Properties of Porous Barium Titanate Ceramics for Biomedical Applications

Karianne Skaar Fedje

Chemical Engineering and Biotechnology

Submission date: June 2017

Supervisor: Mari-Ann Einarsrud, IMA

Co-supervisor: Julia Glaum, IMA

Norwegian University of Science and Technology
Department of Materials Science and Engineering

Preface

This master thesis was carried out at the Department of Materials Science at the Norwegian University of Science and Technology (NTNU) as a part of the study program Chemical Engineering and Biotechnology. The work was carried out from January to June 2017. Professor Mari-Ann Einarsrud and Postdoctoral fellow Julia Glaum have supervised this work. This thesis is a continuation of the compulsory specialization project titled "*Study of Electric Poling Behaviour of Porous Barium Titanate Ceramics*" [1], carried out during the fall 2016.

Numerous people have provided their assistance to this master thesis. First of all, I would like to thank my supervisors, Postdoctoral fellow Julia Glaum and Professor Mari-Ann Einarsrud for their advice, feedback and support during this semester. I would especially thank Julia Glaum for her invaluable help and guidance with the experimental work. I would also like to thank the technical staff at the Department of Materials Science and Engineering for their training and assistance in the laboratories. Finally, I would like to thank all members of the Inorganic Materials and Ceramics Research Group for fruitful discussions, asking good questions and making me reflect on results.

Trondheim, 2017-06-16

Karianne Skaar Fedje

Abstract

Throughout the last decades, the development of bioactive materials to be used as bone implants has been a very active research area. The number of surgeries related to bone implants are steadily increasing, such that improvements in this field are for the benefit of more and more people. However, bone implants used today require long recovery time and aseptic loosening is a commonly occurring issue. By using an active material with the ability to mimic the natural mechanisms of bone regeneration, the healing process might be improved and the recovery time decreased. The mechanisms of bone regeneration are rather complex and involve, among other factors, the response of bone forming cells to mechanical triggers and electrical stimuli.

The bone regeneration is activated by an electric potential occurring in the bones upon application of a mechanical stress, similar to the piezoelectric effect.

Recent investigations of porous implant materials shows that large, interconnected pores allow ingrowth of vascularized cells, and hence increase the interface stability between the bone and the implant.

Barium titanate (BaTiO_3) has been suggested as a potential implant material, due to its biocompatibility, piezoelectricity and mechanical properties. However, as the mechanical and piezoelectric properties decrease with increasing porosity, it is of interest to investigate how these relationships change depending on porosity.

Porous samples of BaTiO_3 were made through the sacrificial template method, using corn starch and poly(methylmethacrylate) (PMMA) as pore formers. The

phase purity and microstructure of the samples was characterized by X-ray diffraction (XRD) and scanning electron microscopy (SEM). The piezoelectric coefficient, describing the electrical response of the material to a mechanical stimulus and vice versa, was determined on electrically poled samples. The microhardness of the samples was investigated by Vickers' indentation measurement. In order to estimate how the material retains its piezoelectric and mechanical properties within the body, the properties were measured prior and subsequent to soaking in 0.9% NaCl-solution for 14 days.

Samples made with both pore formers resulted in a homogeneous pore distribution. The samples made with PMMA showed promising qualities in terms of porosity control and piezoelectric properties at porosities up to ~55 vol% of the total volume of the pellet. Interconnected pores within the desired size range were obtained at a porosity of 50 vol% added PMMA, whereas for corn starch the desired pore size was not observed until addition of 80 vol% pore former. The hardness was higher for the samples made from corn starch. However, as the hardness measurements were difficult to conduct, further investigation of the mechanical properties, through nanoindentation or uniaxial compression testing is suggested.

Sammen drag

I løpet av de siste tiårene har utvikling av bioaktive materialer til bruk som beinimplantat vært et aktivt forskningsområde. Antall operasjoner relatert til beinimplantat er økende, og forbedringer innen dette området vil være til nytte for stadig flere. Beinimplantatene som brukes i dag krever lang rekonvalesenstid etter operasjon. I tillegg blir kontaktflaten mellom implantatet og vevet i kroppen slitt over tid, noe som medfører at implantatet kan løsne. Ved å bruke et bioaktivt materiale som etterligner de naturlige mekanismene bak regenerasjon av bein-celler i kroppen, kan det være mulig å senke rekonvalesenstiden. Mekanismene bak regenerasjonen av bein er komplekse og innebærer blant annet beingenererende cellers respons til mekaniske belastning og elektrisk stimulans.

Regenerering av bein aktiveres av et elektrisk potensiale som oppstår under mekanisk belastning av beina, tilsvarende en piezoelektrisk effekt.

Nyere forskning av porøse implantatmaterialer viser at store, sammenhengende porer tillater vekst av vaskulære celler inn i implantatet og dermed øker stabiliteten ved kontaktflaten.

Barium titanat BaTiO_3 er foreslått som et potensielt implantatmateriale, grunnet materialets biokompatible, mekaniske og piezoelektriske egenskaper. Ettersom mekaniske og piezoelektriske egenskaper minker med økende porøsitet i materialet, er det ønskelig å undersøke hvordan forholdet endres ved økt porøsitet.

Porøse prøver av BaTiO_3 ble laget ved å bruke to ulike poreformere, maisstivelse og polymetylmetakrylat (PMMA). Faserenheten og mikrostrukturen til materialet ble undersøkt ved røntgendiffraksjon og scanning elektronmikroskopi.

Den piezoelektriske koeffisienten ble funnet ved målinger av elektrisk polede prøver. Mikrohardheten av de porøse prøvene ble undersøkt ved Vickers hardhetstest. For å få en indikasjon på hvorvidt egenskapene til materialet forblir de samme etter implantasjon, ble de piezoelektriske og mekaniske egenskapene undersøkt før og etter å ha vært nedsenket i 0.9% NaCl-løsning i 14 dager.

Prøver laget med begge poreformerne resulterte i en mikrostruktur med homogen distribusjon av pore. Prøvene som ble laget med PMMA gav god kontroll over porøsiteten og hadde lovende piezoelektriske egenskaper opp til porøsiteten nådde ~55 vol%. Sammenhengende porer innen ønsket størrelse ble funnet i prøver med 50 vol% tilsatt PMMA. For prøver laget med maisstivelse ble tilsvarende størrelse på porene oppnådd ved tilsetning av 80 vol% poreformer. Hardheten var høyere for prøver laget med maisstivelse. Ettersom hardhetsmålingene hadde store usikkerheter, anbefales videre undersøkelse av mekaniske egenskaper ved kompresjonstesting.

Contents

Preface	i
Abstract	iii
Sammendrag	iv
1 Background	1
1.1 Motivation	1
1.2 Aim of the work	3
2 Introduction	5
2.1 Mechanical properties	5
2.1.1 Mechanical properties of ceramics	6
2.1.2 Mechanical properties of bone	7
2.2 Piezoelectricity	8
2.2.1 Ferroelectricity	10
2.2.2 Stress generated potentials in bone	11
2.3 Processing of porous ceramics	13
2.3.1 Sintering of porous ceramics	15
2.4 Material system - BaTiO ₃	16
2.4.1 Crystal structure	16
2.4.2 Mechanical properties	16
2.4.3 Electric properties	17

2.4.4	Biocompatibility, toxicity and solubility	18
2.5	Electric poling	19
2.5.1	The effect of porosity, pore size and pore shape	19
2.5.2	The effect of an internal bias field	21
3	Experimental	23
3.1	Sample processing	23
3.1.1	Powder preparation	25
3.1.2	Addition of pore former	25
3.1.3	Sintering	26
3.2	Sample characterization	27
3.2.1	Phase purity	27
3.2.2	Porosity measurements	28
3.2.3	Microstructure	28
3.3	Piezoelectric measurements	29
3.3.1	Exposure to saline environment	30
3.4	Hardness measurements	31
3.4.1	Exposure to saline environment	31
4	Results	33
4.1	Phase purity	33
4.2	Porosity	34
4.3	Microstructure	37
4.3.1	The effect of calcination temperature	37
4.3.2	The effect of mixing	38
4.3.3	The effect of pore former	39
4.4	Piezoelectric properties	41
4.5	Hardness	44
5	Discussion	47
5.1	Microstructure	47
5.1.1	The effect of pore former shape on interconnectivity	47
5.1.2	The effect of pore size and shape on shrinkage during sintering	49

5.1.3	The effect of mixing procedure	50
5.2	Electric poling and piezoelectric properties	50
5.2.1	The effect of pore former and amount	51
5.2.2	The effect of soaking	52
5.3	Mechanical properties	53
5.3.1	The effect of pore former and amount	54
6	Conclusion	57
7	Further work	59
A	Additional X-ray diffractograms	61
B	Density plots	63
C	Additional SEM-images	67
D	Additional hysteresis loops	71
E	Table mechanical testing	75
F	Sample overview	77
	References	79

Chapter 1

Background

1.1 Motivation

Bone is a complex biomaterial with the ability to regenerate itself. However, some fractures are too severe to be fixed by the self-healing process. These fractures are repaired by the use of an implant material, which works as a replacement of the damaged bone. The need for implant materials are constantly increasing with the aging population, as elderly people are more prone to bone fracture.

Implant materials commonly used today are metals and metal alloys, such as titanium and stainless steel [2]. The mechanical properties of these materials make them suitable for replacement of bones. However, the recovery time after surgery is long and aseptic loosening is a commonly occurring issue after the material has been implanted for a while [2]. Several revision surgeries are therefore often necessary, leading to even longer leave from work and reduced quality of life for the patients. This is not only an issue for the patients, but also costly for the community [2, 3].

For these reasons, the search for a new and improved bone implant material has been an important research field. Several material systems have been suggested for the use as bone implant, such as polymers [4] and porous piezoelectric ceramics [5, 6].

The formation of a stable interface between the living bone and the artificial implant heavily depends on the attachment and ingrowth of bone and vascular cells. To be able to form a vascularized structure within an artificial material, pores of sizes larger than 100 μm are needed [7, 8]. The ingrowth of cells and

creation of living bone inside the pores, will lead to a better attachment and hence increase the interface stability. This is believed to decrease the occurrences of aseptic loosening [8].

Bone regeneration is a complex process which is governed by several mechanisms. Modern implant materials aim to mimic the processes found in bone to promote bone cell growth. This can be done by coating the implants with growth factors or by roughening the surface of the implant in order to increase cell adherence [9]. One mechanism discussed as being important for bone healing is the electric potential observed in load bearing bones, which is generated upon application of mechanical stress. This process can be mimicked by using a piezoelectric implant material. In combination with a porous structure, this could be beneficial for the bone healing and reliability of an implant [8].

Besides the structural and piezoelectric characteristics, the mechanical properties of a potential implant material are also of importance, as differing elastic properties might lead to stress shielding and degradation of the living bone. It is therefore important that the mechanical properties of the implant material match the mechanical properties the tissue where it is implanted [8].

1.2 Aim of the work

Barium titanate (BaTiO_3) is a biocompatible piezoelectric ceramic with mechanical properties similar to the mechanical properties of bone. This makes BaTiO_3 a promising material for scaffold engineering.

This thesis aims to reveal the connection between porosity, piezoelectric and mechanical properties of BaTiO_3 ceramic. As piezoelectric properties were reported to decrease with increased porosity [10], it is of particular importance to study this dependency upon introduction of controlled porosity over a broad porosity range. This will be done by investigating the piezoelectric properties of the final porous ceramic, made with a controlled amount of added porosity.

Piezoelectric materials, such as BaTiO_3 , have to be electrically poled in order to achieve a macroscopic piezoelectric effect. Poling is a challenge when it comes to porous materials, as the electric field is enhanced in the areas surrounding the pores. The shape of the pores are an important factor when it comes to electric field enhancement. Dielectric breakdown during poling occurs more often in porous materials with irregular shaped pores than spherical pores [10]. The effect of size and shape of the pore former on the final piezoelectric measurement is therefore of interest to investigate. This will be done by making samples using two different pore formers, corn starch, giving irregular pores, and poly(methylmethacrylate) (PMMA), leading to spherical pores.

Porous materials are more brittle than dense materials [11]. It is of interest to examine how much porosity can be introduced to the samples before they get too brittle to be used as a bone substitute. This will be investigated, by measuring the hardness of samples of different porosity.

As the material will be implanted to the body, it is of importance to examine if the material will retain its properties after being exposed to the environment in the body. This will be done by measuring the piezoelectric and mechanical properties of the samples before and after soaking in saline solution at 37°C for a period of 2 weeks. The results from this thesis will form a database to build on for future research.

Chapter 2

Introduction

2.1 Mechanical properties

In order for a material to function as a bone replacement it has to have mechanical properties that match the properties of the tissue where it is implanted [12]. Investigation of the mechanical properties of a potential bone implant material is therefore highly important. Hardness, compressive strength and elasticity are especially interesting properties to investigate, as the implant material has to be able to bear the load of the body without breaking or being deformed. The values of these properties should also be as similar to bone as possible to reduce the chance of loosening and to avoid stress shielding, which could lead to loss of bone density [8].

Vickers' indentation test is commonly used to determine the hardness of a material. This test gives the microhardness, at the area where the indent is made. The hardness, HV, is dependent on the force applied, P, and the diameter of the indent, d_1 , as shown in Equation 2.1.1 [13].

$$HV = 1.854 \frac{P}{d_1^2} \quad (2.1.1)$$

2.1.1 Mechanical properties of ceramics

Most ceramic materials have high hardness, high elastic modulus, E , and no plastic deformation upon application of a load [11]. The lack of plastic deformation leads to brittle fracture.

The mechanical properties of a material are related to the strength of the bonds between the atoms in the material. Some ceramics have weak ionic bonds, which results in a low elasticity modulus. Ceramics with strong covalent bonds, have higher E values [11]. The hardness of a ceramic material also increases with increasing bond strength between the atoms [14]. The elasticity modulus of ceramic materials is generally higher than the corresponding value for cortical bone. The fracture toughness is generally lower for most ceramics, although there do exist some with similar fracture toughness as bone [15]. The fracture toughness of ferroelectric ceramics depend on whether or not the material is poled. For a poled ferroelectric material, the fracture toughness will be anisotropic, with larger values in the direction parallel to the poling direction. This is an effect of domain switching in the area around the crack, impeding crack propagation [16].

Several researchers have examined the relationship between hardness and strength of materials. Various relations have been suggested, however, the relation is different for different types of materials, such as metals and ceramics [17]. Rice *et al.* have suggested the following relation between hardness and microplastic yield stress for ceramic materials [11]:

$$HV = 3 \cdot \sigma_Y \quad (2.1.2)$$

Where HV is the Vickers' hardness, σ_Y is the yield stress. Experimental data from the same research have shown that the compressive strength, σ_c is found within the range given in Equation 2.1.3:

$$\frac{1}{2}\sigma_Y < \sigma_c < \frac{3}{4}\sigma_Y \quad (2.1.3)$$

meaning that there is a linear relation between the hardness and the compression strength of a ceramic material.

Effect of porosity

Cracks, pores and inclusions affect the mechanical properties of ceramic materials. Mechanical stresses are concentrated in the area surrounding a pore, which decreases the strength of the ceramic. Pores with irregular shape will result in a larger stress concentration than a spherical pore. The size of the pore also affects the mechanical properties. With increased pore size, the mechanical properties decrease, as it leads to higher stress concentrations in the material [11].

If the pores in the material are clustered, application of load will lead to cracking in the area between the pores before it occurs in an area with non-clustered pores. This will result in a larger flaw, which reduces the strength of the ceramic.

2.1.2 Mechanical properties of bone

Bone consists of two main parts, the cortical bone and the trabecular bone. The compact cortical bone surrounds the less dense trabecular bone, which has a cellular structure, as shown in Figure 2.1.1 [15]. The cortical bone has a compressive strength of 100-230 MPa and a Young's modulus of 7-30 GPa, while the corresponding values for the trabecular bone are 2-12 MPa and 0.005-0.5 GPa, respectively [15]. This composite structure results in both high strength and bending resistance, as well as low weight. The fracture toughness of bone is 3-6 $\text{MPa}\sqrt{m}$ [18] and the elasticity modulus is 20-30 GPa [19]. The mechanical properties of bone are summed up in Table 2.1.1.

Table 2.1.1: The mechanical properties of bone. σ_c is the compressive strength, E is the elasticity modulus, K_{IC} is the fracture toughness and H represents the hardness of the bone.

	σ_c [MPa]	E [GPa]	K_{IC} [$\text{MPa}\sqrt{m}$]	H [GPa]
Cortical bone	100-230 [15]	7-30 [15]	-	-
Trabecular bone	2-12 [15]	0.005-0.5 [15]	-	-
Combined	-	20-30 [19]	3-6[18]	0.23-0.76 [20]

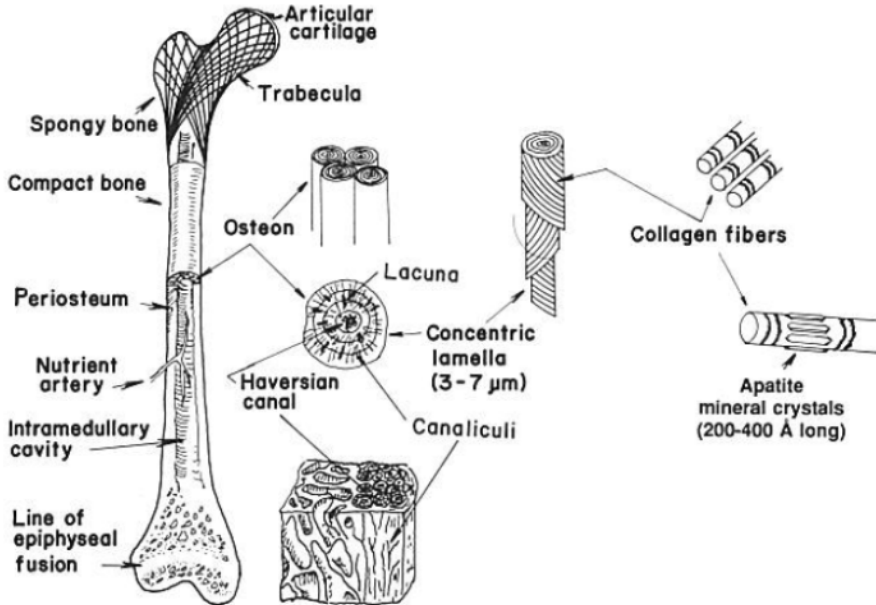


Figure 2.1.1: The figure shows the structure of bone from macrostructure to sub-nanostructure. Figure from Park and Lakes [21]

2.2 Piezoelectricity

Dielectric materials are insulating materials, which will gain a slight polarization upon application of an electric field. The polarization occurs due to a displacement of one of the ions in the crystal structure creating temporary dipoles. In some dielectric materials, the polarization will develop upon application of a mechanical force, resulting in a surface electric charge. These materials are known as piezoelectric materials, and their response to mechanical loading is the direct effect of piezoelectricity [14]. There also exists a converse effect, where a strain in the material occurs upon application of an electric field. The strain can be either tensile or compressive, as shown in Figure 2.2.1.

The piezoelectric coefficient, d , is a third-rank tensor used to describe the piezoelectric properties of a material. The coefficient is used to describe both

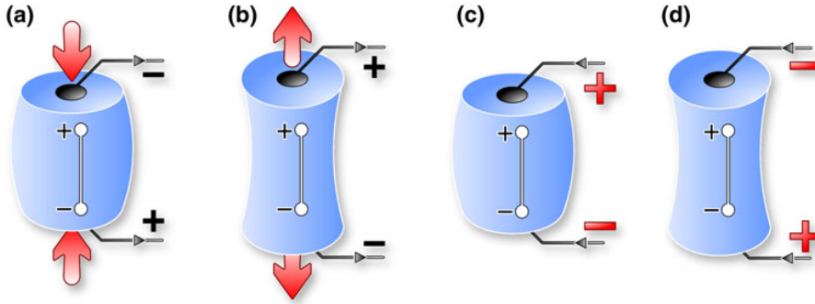


Figure 2.2.1: The direct effect is shown for an applied compressive force (a) and tensile force (b). The converse effect when an electric field parallel to the poling in the material is applied (c) and opposite to the poling in the material (d). Figure from Baxter *et al.* (2010) [22].

the direct and the converse effect. For the direct effect it gives the relationship between the dielectric displacement, D , and the stress applied, T . For the converse effect, it gives the relation between the strain occurring in the material, S , upon application of an electric field, E [23]. The numeric value of d is identical for the direct and the converse effect, as shown in Equation 2.2.1.

$$d = \frac{D}{T} = \frac{S}{E} \tag{2.2.1}$$

d_{33} is the piezoelectric coefficient when the strain is measured along the same axis as the electric field is applied.

2.2.1 Ferroelectricity

Piezoelectric materials with an ability to be spontaneously polarized are called pyroelectric materials [14]. Ferroelectric materials are a subgroup of pyroelectric materials, where the spontaneous polarization can be reversed upon the application a certain electric field, the coercive field, E_C .

Ferroelectric materials display several ferroelectric domains [24]. Within each domain, the displacement of the ion causing the polarization occurs in the same direction, resulting in a net dipole moment of each domain. The net polarization of the ferroelectric material is the sum of dipole moments in each domain [14]. The net dipole moment of an unpoled ferroelectric material is zero, as the material consists of several ferroelectric domains with different orientations.

Upon application of an electric field, switching of the ferroelectric domains and growth of domains with favourable orientation occurs. The result is alignment of the domains, causing a non-zero net dipole moment in the material [25].

When the domains are aligned as good as possible, considering grain orientation and constraints between grains, the polarization of the material is saturated, marked as point C in Figure 2.2.2. The remanent polarization, P_r , is the polarization remaining in the material after application of an electric field. In this state, some of the ferroelectric domains will have switched back to their original state. As the majority of the domains remain aligned, the material will still retain a net dipole moment [24]. The remanent polarization (point D and H, Figure 2.2.2) is particularly interesting in the case of implant materials, as there it gives the characteristic value retained without application of an electric field, which will be the case when implanted in the body.

The alignment of the ferroelectric domains in the remanent state, as well as how easy the domains can be reoriented by an electric field or mechanical stress, determines the piezoelectric properties of a material.

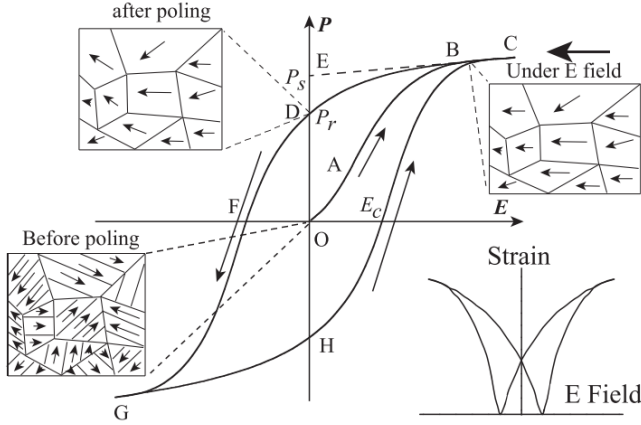


Figure 2.2.2: The hysteresis loop of a ferroelectric material. Before the poling, the ferroelectric domains are randomly distributed throughout the material. At point B, the material is affected by the electric field, resulting in domain alignment. P_s indicated the saturated polarization. P_r marks the remnant polarization, where the applied electric field is zero. E_c shows the coercive field of the material. Figure from Jin *et al.* (2014) [26].

2.2.2 Stress generated potentials in bone

Stress generated potentials, similar to the piezoelectric effect, were discovered in bone in 1954 [4]. This potential has proven to be an important factor for bone growth, as it activates the osteoblasts, the bone generating cells. A combination of several responses in the body are responsible for the potential difference, making it a complex mechanism [27]. Research has shown that both the properties of collagen fibres and streaming potentials across the bone play an important role in generating the electric potential [4].

Collagen fibres are one of the main constituent of the bone. The fibres consist of several triple helices of amino acids, as shown in Figure 2.2.3 [4]. Hydrogen bonds stabilize the triple helices and aligns the amino acid backbones, which have a dipole moment. The alignment causes a net permanent polarization of the collagen fibres [4]. The polarization of the collagen fibre has been discussed as one important factor behind the piezoelectric response in bone [28, 29]. Studies

of piezoelectric properties of collagen fibrils show that there is a response along the fibril axis. A piezoelectric coefficient of 1 pm/V has been reported for a single collagen fibre [28].

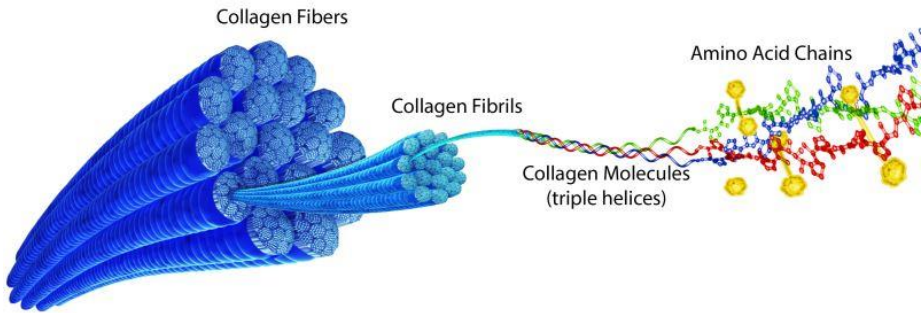


Figure 2.2.3: The figure shows the structure of collagen from fibre to amino acid chains. The figure is extracted from the webpage of HarbourMedTech with permission [30].

The collagen fibrils contain hydroxyapatite particles, that have proven to increase the surface charge density of the collagen fibrils [31]. This results in an increased zeta potential and hence an increased streaming potential of the interstitial fluid in the bone [27], as shown in Figure 2.2.4. Investigations on the effect of streaming potentials in bone have shown that the fluid flow initiates the generation of new bone cells [27]. The streaming potential is a function of pressure applied to the fluid and will be present without the enhancement by hydroxyapatite. It is therefore suggested that the stress generated potentials in bone is a combination of the alignment of collagen fibres, surface charge enhancement by hydroxyapatite and the streaming potential.

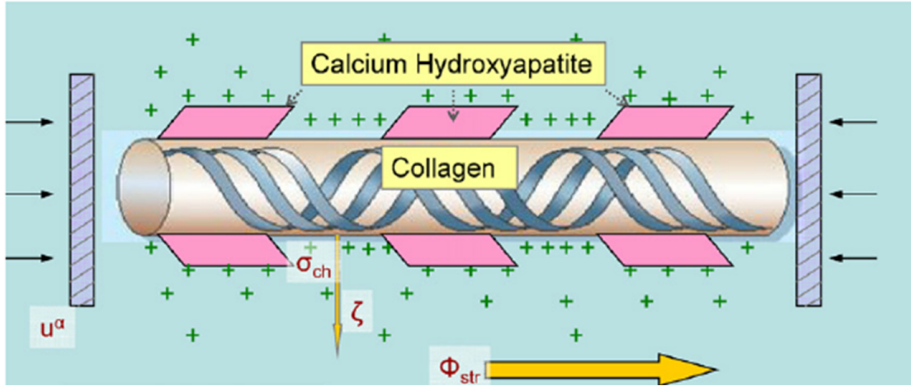


Figure 2.2.4: The figure shows the mechanism occurring in bone upon application of mechanical stress. u^a represent the displacement, σ_{ch} is the surface charge, ζ is the zeta potential and Φ_{str} represents the streaming potential. The figure is adjusted from a figure by Ahn *et al.* (2009) [27].

2.3 Processing of porous ceramics

The usage of porous implant materials is thought to increase the stability of the interface between the implant and the surrounding tissue [32]. A material with large, open porosity allows in-growth of new bone tissue into the implant. Interconnected pores with a pore size of at least 100 μm in diameter is required to allow tissue ingrowth into the implant [7, 33]. There are several processing techniques used for making porous ceramic materials, resulting in different pore structures. The three most common are the replica technique, the direct foaming method and the sacrificial template method.

The replica technique uses cellular structures, such as sponges, that are covered in ceramic suspension. Large pores in the cellular structure are required, in order to be able to coat the entire surface of the structure. The ceramic is dried at temperatures as low as room temperature, before the cellular structure is burnt off by slow heat treatment, resulting in a ceramic material with large pores [34]. Reported sizes of pores in the final structure are within the range of 200 μm -3mm [35]. The shape of the pores will depend on the structure of the sponge.

When using the indirect foaming method, air is incorporated into a ceramic suspension, creating air bubbles. The consolidated foams are sintered, resulting in a highly porous ceramic. Final pore sizes within the range of $35\ \mu\text{m}$ - $1.2\ \text{mm}$ have been reported [35]. Pores of a size smaller than $200\ \mu\text{m}$ can be achieved by adding chemical reactants to increase the consolidation process. When using this method, the porosity of the sintered ceramic will be equal to the amount of gas added to the ceramic suspension during foaming. The final pore shape is usually spherical [35].

The sacrificial template method is based on mixing the ceramic precursor powder with a sacrificial phase. The goal of the mixing is to achieve a homogeneous distribution of the secondary sacrificial phase in the precursor powder [35].

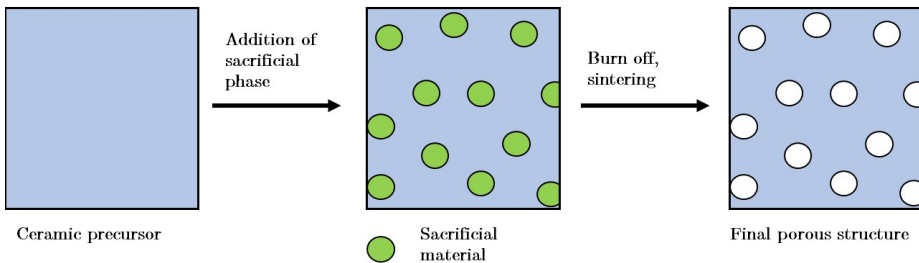


Figure 2.3.1: The figure shows the procedure of the sacrificial template method where a sacrificial phase is added to a ceramic precursor, then burnt off.

The sacrificial powder is burnt off prior to sintering, resulting in a ceramic with homogeneously distributed pores, as shown in Figure 2.3.1. The final pore size and shape will depend on the size and shape of the sacrificial template used. Porosities from $1\text{-}700\ \mu\text{m}$ have been achieved by using this method. This method gives the possibility to tailor the microstructure in terms of pore size, shape, and distribution [35]. In this thesis, the sacrificial template method is used.

2.3.1 Sintering of porous ceramics

Sintering is a densification process of ceramic materials by heat treatment. Several mechanisms for material transport occur during the sintering, some leading to densification, others to coarsening of particles and grain growth. The driving force for densification is reduction of surface free energy by reducing the surface area [36].

The conventional sintering process can be divided into three steps. In the initial stage, the particles are in contact after being formed into a green body with the desired shape, often by pressing. In the intermediate stage, a neck forms between the particles by lattice diffusion, surface diffusion and vapor transport. The densification occurs in the final stage, when the distance between the centres of two particles decrease due to grain boundary diffusion and lattice diffusion through the grain boundary.

When using the sacrificial template method, the pore former is burnt off prior to sintering, leaving pores where there previously was organic matter, as shown in Figure 2.3.1 [10]. The pores affect the densification process during sintering [37, 38]. Experiments conducted with organic pore formers show that the pore shape usually remains the same after sintering, but the size decreases, due to shrinkage during sintering [37–40]. This means that spherical pore formers usually result in spherical, closed pores, while irregular shaped pore formers result in more interconnected pores. If the size of the pore former is very different from the grain size of the ceramic, it can make the mixing more difficult. However, if the size of the pore former approaches the grain size of the ceramic powder, the chances of intergranular cracking increases [11]. Cracking could also occur if there is a mismatch between the thermal expansion coefficient of the powder and the sacrificial template [35].

2.4 Material system - BaTiO₃

Barium titanate (BaTiO₃) is a ferroelectric ceramic material [23] with low toxicity [41], high strength and low adsorption of water [33], properties proven to be important for scaffold engineering [4].

2.4.1 Crystal structure

BaTiO₃ has a perovskite crystal structure, where the Ba²⁺-ions create a cubic unit cell, with O²⁻-ions in the face centres and the Ti⁴⁺-ions filling the octahedral holes. Upon cooling of the material below the Curie temperature ($T_c \sim 130^\circ\text{C}$) the unit cell transforms to a tetragonal phase, with an elongated c-axis [14]. As the Ti⁴⁺-ion is too small to fill the octahedral holes completely, a displacement of the Ti⁴⁺-ion towards one of the O²⁻-ions will occur, as shown in Figure 2.4.1.

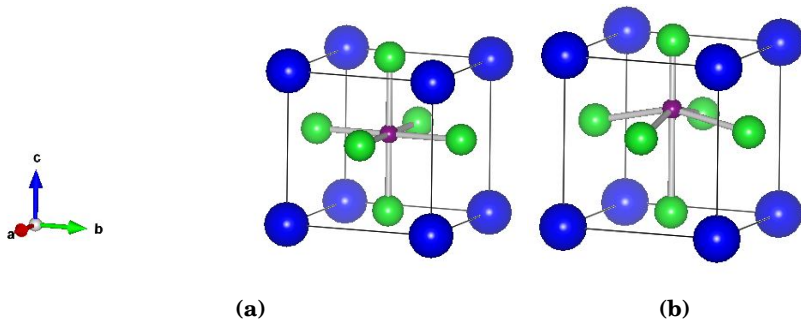


Figure 2.4.1: (a) Cubic perovskite unit cell of BaTiO₃. (b) Tetragonal structure of BaTiO₃ where the Ti⁴⁺-ion is displaced along the elongated c-axis. The blue spheres represent the Ba²⁺-ions, the green represent the O²⁻-ions and the purple represent the Ti⁴⁺-ion. The figure has been made using VESTA-software.

2.4.2 Mechanical properties

As addressed in Section 2.1, the mechanical properties of a potential bone implant material are highly important. Properties such as strength and hardness need to be of a certain value in order to function as a replacement for bone.

BaTiO_3 has a hardness of 5.2 GPa [42] and an elasticity modulus of 99 GPa [43]. The mechanical properties of BaTiO_3 are summed up and compared to the mechanical properties of bone in Table 2.4.1.

The fracture toughness of $\sim 2 \text{ MPa}\sqrt{m}$ [44] is quite close to the fracture toughness of bone ($3\text{-}6 \text{ MPa}\sqrt{m}$ [18]). However, porosity has a large effect on the mechanical properties of ceramics, as addressed in Section 2.1.1. It is therefore of interest to investigate how these properties change upon increased porosity.

Table 2.4.1: The mechanical properties of dense BaTiO_3 is given in the table. σ_c is the compressive strength, E is the elasticity modulus, K_{IC} is the fracture toughness and H represents the hardness of the material. Corresponding values for bone are given for comparison.

	σ_c [MPa]	E [GPa]	K_{IC} [$\text{MPa}\sqrt{m}$]	H [GPa]
BaTiO_3	100 [44]	99 [43]	~ 2 [44]	5.2 [42]
Cortical bone	100-230 [15]	7-30 [15]	-	-
Trabecular bone	2-12 [15]	0.005-0.5 [15]	-	-
Combined	-	20-30 [19]	3-6[18]	0.23-0.76 [20]

2.4.3 Electric properties

As addressed in Section 2.2.2, stress generated fields activate the bone regenerating cells. The generation of electric fields upon application of pressure is similar to the effect found in piezoelectric materials. As a piezoelectric material with d_{33} of 191pC/N [23], BaTiO_3 is believed to increase the bone regrowth after implantation. This makes it a potential bioactive material, as it will participate in the processes taking place in the body by actively stimulate the bone regeneration.

As a ferroelectric material, BaTiO_3 will become polarized upon application of an electric field, due to domain alignment and movement of domain walls, as described in Section 2.2.1 [24]. A dense BaTiO_3 ceramic has a coercive field of $\sim 100 \text{ V/mm}$ [45]. The low coercive field makes it possible to pole the material in

air, as it is far from the electric breakdown field of air (1 kV/mm).

BaTiO₃ has a high dielectric constant, K . Values as high as 1400 have been measured for the dielectric constant of BaTiO₃ [23]. Some of the electric properties of BaTiO₃ are summed up in Table 2.4.2.

Table 2.4.2: Electric properties of dense BaTiO₃. d_{33} is the piezoelectric coefficient, P_s is the saturation polarization, E_c is the coercive field, K is the relative dielectric coefficient in an unpoled state and T_c is the Curie temperature.

	d_{33} [pC/N]	P_s [C/m ²]	E_c [V/mm]	K [-]	T_c [°C]
BaTiO ₃	191 [23]	0.26 [24]	100 [45]	1400 [23]	~130 [23]

2.4.4 Biocompatibility, toxicity and solubility

A potential bone implant material has to be biocompatible, meaning that it has to be able to conduct the task it is designed to do in the body, without doing any harm. Some piezoelectric ceramics, such as lead zirconate titanate (PZT), have good piezoelectric properties, but are toxic, and can for that reason not be used as a bone implant. Solubility in saline solution is another issue with many piezoelectric ceramics. As ceramic material consists of ions, it is often soluble in water, which can result in ion release over time. Release of ions will not only lead to degradation of the implant material, in some cases, the released ions can be detrimental to surrounding cells [7]. Results from previous research on the biocompatibility of BaTiO₃ shows that the material has promising qualities as a bone implant material [6, 32, 33, 41, 46, 47]. As reported by Yu, W. *et al.* (2011), BaTiO₃ has low toxicity and no release of ions in a saline environment resembling the environment of the human body [41]. Results from *in vitro* experiments conducted on mice osteoblast cells show no significant inflammatory response in the cells upon exposure to BaTiO₃ [46].

An implant material must also retain its properties over time after implantation. In the study conducted by Yu *et al.* (2011), BaTiO₃ was exposed to a saline solution, resembling the environment in the body, for 28 days. The study

showed that the material retained important properties, such as biaxial strength and piezoelectric coefficient [41].

By using a bioactive material as a bone implant, the material should participate in regeneration of bone cells. *In vivo* experiments conducted by Park *et al.* showed an increased cell regrowth in the area where BaTiO_3 was implanted compared to the area around an electrically inactive implants [32]. Similar results were found when a composite of hydroxyapatite and BaTiO_3 (HABT) was implanted into jawbones of dogs. The bone regeneration in the area around the HABT-implant was promoted compared to the bone generation around an implant made of pure hydroxyapatite [6].

2.5 Electric poling

In order to take advantage of the piezoelectric properties of a ferroelectric material, the material has to be electrically poled. As described in Section 2.2.1, alignment of the ferroelectric domains occurs during poling in an electric field. Upon investigation of potential active bone implant materials, the remanent piezoelectric properties are of interest, as these are the properties the material will retain subsequent to poling. As the remanent piezoelectric properties of a material are related to the domain configuration after electric poling, it is of importance to examine and optimize the poling behaviour of porous piezoelectric ceramics.

2.5.1 The effect of porosity, pore size and pore shape

The electric poling behaviour of a material is strongly related to the microstructure of the material. Pores affect the movement of the electric field lines, locally enhancing the electric field, as shown in Figure 2.5.1. These local electric fields can be higher than the field applied externally [48–50].

Several researchers have investigated the effect of porosity, pore size and shape on the electric poling behaviour of porous piezoelectric ceramics. Experiments have been conducted with both lead zirconate titanate (PZT) [10] and lithium sodium potassium niobate (LNKN) [38], using two different pore for-

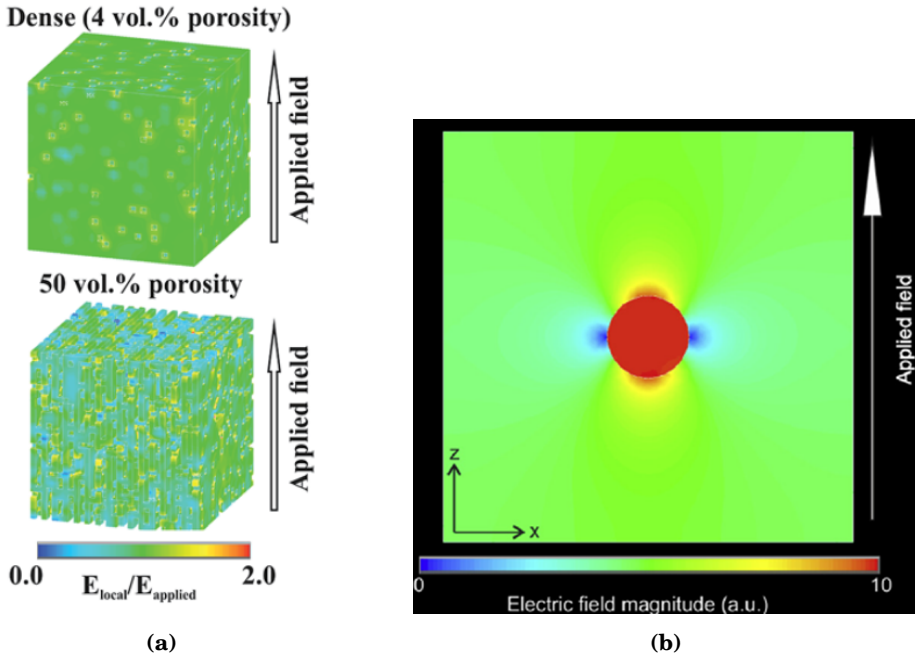


Figure 2.5.1: Figure (a) shows finite element method (FEM) model of how the electric field is distributed in a dense and a porous material. Figure from Zhang *et al.* (2014) [50]. Figure (b) shows a FEM-model of how the electric field is distributed around a spherical pore. Figure from Roscow *et al.* (2017) [48].

mers; one giving spherical pores and the other more irregular, interconnected pores. Both experiments showed a clear trend of decreasing piezoelectric properties with increased porosity. The effect of pore size and shape was not as coherent. The results from the research on porous PZT showed that the samples with spherical pores obtained better piezoelectric properties than samples with irregular shaped pores. The experiment conducted with LNKN showed the opposite, most likely due to flaws found on the walls of the pores arising from thermal expansion of the spherical pore former during sintering [38].

Porosity also increase the probability of dielectric breakdown, due to the low dielectric strength of air inside the pores. Spherical pores are favourable for this

reason, as irregular pores lead to a stronger field intensification, which can lead to dielectric breakdown. However, for bone implant applications interconnected pores are more favourable, as they allow tissue ingrowth, which will stabilize the interface between the implant and the bone [3, 7]. These aspects have to be balanced in the development of a potential bone implant material.

2.5.2 The effect of an internal bias field

The piezoelectric properties of a material can also be negatively affected by electric poling. If the material is poled for a longer time, an internal bias field can develop. This is due to charge carrier migration towards, and accumulation at the grain boundaries. This results in a horizontal shift in the polarization hysteresis loop in the opposite direction of the internal bias field, as shown in Figure 2.5.2. The internal bias field becomes large with respect to the coercive field of the material, causing bias ferroelectric switching from the aligned state and hence, decreases the piezoelectric properties [25].

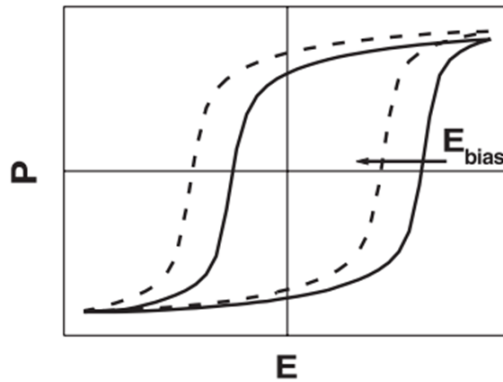


Figure 2.5.2: The figure shows the hysteresis loop for a piezoelectric material. The stippled line shows the hysteresis loop of a sample with no internal bias field. The solid line shows the hysteresis loop of a sample where an internal bias field has developed, resulting in a horizontal shift of the loop. Figure from Balke *et al.* (2007) [51].

Chapter 3

Experimental

3.1 Sample processing

BaTiO₃ was made from oxide and carbonate precursor powders through the solid-state route. Corn starch and poly(methylmethacrylate) (PMMA) was used as pore forming agents to introduce controlled porosity to the samples. Materials used for synthesis and characterization are given in Table 3.1.1.

Table 3.1.1: Materials used in sample preparation.

Name	Chemical formula	Supplier	Purity [%]
Barium Carbonate	BaCO ₃	Sigma-Aldrich	≥ 99 ¹
Barium Carbonate	BaCO ₃	Sigma-Aldrich	99.98 ²
Titanium(IV) oxide, rutile	TiO ₂	Sigma-Aldrich	99.99
Corn starch	(C ₆ H ₁₀ O ₅) _n	Carl Roth	-
Poly(methylmethacrylate) (PMMA)	CH ₂ C(CH ₃)	Acros Organics	-
Ethanol	C ₂ H ₆ O	VWR International AS	96
Isopropanol	C ₃ H ₈ O	VWR International AS	-
Salt water solution	NaCl + H ₂ O	B. Braun	0.9

¹ Was used for the calcination test and the first two batches of calcined powder

² Was used for the remaining calcination batches

The apparatus used for both synthesis and characterization are summed up in Table 3.1.2.

Table 3.1.2: Apparatus used for synthesis and characterization.

Apparatus	Model	Application
Ball mill	U.S. Stoneware	Mixing and milling of powders
Rotary evaporator	Buchi Rotavapor R-210	Evaporation of ethanol from wet powder
Furnace	Nabertherm P330	Calcination, Starch burn-off
Clean furnace	Narbertherm P330	Sintering, thermal etching
Grinder	Struers LaboPol-21	Grinding samples
Polisher	Struers Tegramin 20	Polishing samples
XRD	Bruker D8 Advance daVinci	Analyzing phase composition
Carbon coater	Cressington 208	Coating of pellets prior to SEM-analysis
Sputter coater	Edwards sputter S150B	Application of Au-electrodes
SEM	Hitachi S-3400N	Investigation of micro-structure, EDS-analysis
High voltage set-up	aixACCT TF Analyser 2000E	Electric poling, piezo-electric measurements
Macro-indentation	DVK-1S Matsuzava ¹	Measuring hardness of the samples
Macro-indentation	Innovatest Holger X Hartmann ²	Measuring hardness of the samples
Macro-indentation	LEICA VMHT MOT ³	Measuring hardness of the samples

¹ Used for the first hardness measurement

² Used for hardness measurement 2-4

³ Used for hardness measurement 5-7

3.1.1 Powder preparation

A fine powder of BaTiO_3 was produced through solid-state synthesis, by mixing BaCO_3 and TiO_2 . The precursors were dried at $\sim 100^\circ\text{C}$ for 24 hours prior to mixing to evaporate water. The powders were stoichiometrically mixed, with a 1:1 ratio. The precursor powders were mixed in a 6 cm \varnothing plastic container, using a U.S. Stoneware ball mill. Ethanol was used as a solvent and milling balls of yttrium stabilized ZrO_2 were used. The powders were mixed for 24 hours with a rotational speed of 205 rpm.

Subsequent to mixing, the solvent was evaporated using a Buchi Rotavapor R-210. The dry powder was manually ground using a pestle and mortar. Particle size was screened out using a 250 μm sieve. The powder was pressed into pellets of 15 mm \varnothing using a uniaxial press and a pressure of 20 MPa. An experiment to optimize the calcination temperature was conducted by examining the microstructure of dense pellets made from powder calcined at 800, 850, and 900°C. Based on the results from the experiment, a calcination temperature of 800°C was chosen as the optimized temperature. The pellets were calcined in air for 8 hours. A heating rate of 200°C/h was used.

The calcined pellets were crushed and milled, using the same procedure as prior to calcination. The calcined powder was ground and sieved in the same way as after the first milling step.

3.1.2 Addition of pore former

To introduce porosity into the ceramics, organic pore formers of different volume fractions were added to the calcined powder. Two batches were made, one using corn starch ($(\text{C}_6\text{H}_{10}\text{O}_5)_n$) as pore former and one using PMMA ($\text{CH}_2\text{C}(\text{CH}_3)$). Pellets with 0-80 vol% added pore former were made. The pore former and BaTiO_3 were weighed out, using a scale with 5 decimals accuracy.

BaTiO_3 -powder and corn starch were mixed in a dispersion of ethanol, using an ultrasonic bath for 30 minutes. The ethanol was removed by evaporation, using a hot plate at a temperature of 70°C. A magnetic stirrer was used during evaporation, to maintain a homogeneous mix of the powder and pore forming

agent. A rotational speed of 200 rpm was used for this purpose. The same procedure was used for mixing the BaTiO_3 and PMMA with volume fractions from 10-40 vol%. As the PMMA particles formed agglomerates at elevated temperature and high volume fractions, volume fractions of 50-80 vol% PMMA was dry-mixed with BaTiO_3 by manually shaking. The final processing route for making the pellets is shown in Figure 3.1.1. A table giving the processing parameters for all pellets made can be found in Appendix F.

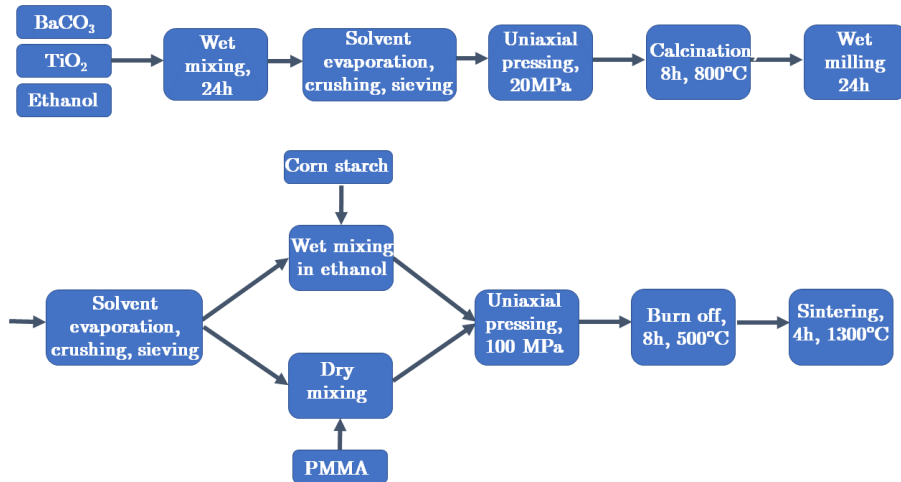


Figure 3.1.1: Flowchart showing the steps of the processing route, from precursor powders to dense pellet. A heating and cooling rate of $200^\circ\text{C}/\text{h}$ was used for all heat treatment steps.

3.1.3 Sintering

As the different measurements to be conducted require differently sized pellets, two different sizes were made. All pellets were made by applying a pressure of 100 MPa, using a uniaxial press.

For the piezoelectric measurements, 5 pellets with a 10 mm diameter were made for each porosity. Two pellets of each porosity was made for the hardness

test, with a diameter of 15 mm.

Three pellets were placed in a Al_2O_3 -crucible, on a layer of sacrificial powder. The pellets were covered in sacrificial powder. An Al_2O_3 lid was placed on top of the crucible, leaving a small gap for evaporation of gasses and supply of oxygen. The pore former was burnt off at a temperature of 500°C for 8 hours. A heating rate of 200°C/h was used for this purpose. The pellets were furthered sintered at 1300°C for 4 hours. A heating and cooling rate of 200°C/h was used. The heating programs used for sample processing are summed up in Table 3.1.3

Table 3.1.3: Heating programs used for sample preparation

Purpose	Heating rate [$^\circ\text{C/h}$]	T [$^\circ\text{C}$]	Holding time	Cooling rate [$^\circ\text{C/h}$]
Calcination	200	800	8 hours	-
Burn-off	200	500	8 hours	-
Sintering	200	1300	4 hours	200
Thermal etching	200	1250	5 minutes	200

3.2 Sample characterization

The sample characterization of the pellets involved investigation of phase purity, microstructure and porosity. The microstructure and phase purity of the samples was investigated using scanning electron microscopy (SEM) and X-ray diffraction (XRD). The porosity of the samples was calculated from Archimedes' method and from measured dimensions.

3.2.1 Phase purity

The phase purity of the calcined powder was investigated by X-ray diffraction (XRD), using Bruker 8 Advanced DaVinci. The powders were scanned for 60 minutes using $\text{Cu-K}\alpha$ -radiation. A 2θ angular range of 20° - 80° was examined using a step size of 0.010° . The data was analyzed using the software Diffraction.EVA

V4.2. One sintered pellet was crushed to powder and examined using the same parameters.

3.2.2 Porosity measurements

The green body density of the pellets was calculated from measured volume and weight. The dimensions of the pellets were measured using a caliper and a scale with four decimals accuracy. The total porosity of the sintered pellets was determined by Archimedes' method, using isopropanol as immersion liquid. The total porosity of the samples, P was calculated using Equation 3.2.1.

$$P = \frac{\rho_t - \rho_b}{\rho_t} \cdot 100\% \quad (3.2.1)$$

Where ρ_t is the theoretical density and ρ_b is the measured bulk density of the sample. Five or six pellets were made for each porosity. The reported density is the average value calculated from all pellets with one porosity. The results are given with errorbars, which give the standard deviation of the values obtained for all pellets with the same amount of added pore former.

3.2.3 Microstructure

The microstructure of the sintered pellets were investigated using scanning electron microscopy (SEM) (Hitachi S-3400N).

In preparation for SEM-analysis, the pellets were polished down to 3 μm grid, using DiaPro Dac-3, a diamond suspension. The pellets were cleaned in ethanol in an ultrasonic bath for 10 minutes to remove solid particles from the polishing. The dense pellets were thermally etched at 1250°C for 5 minutes, using a heating and cooling rate of 200°C. This was done in order to examine the grain boundaries of the sample. Prior to the analysis, all samples were coated with carbon, using Cressington 208 Carbon coater.

3.3 Piezoelectric measurements

As BaTiO_3 is a non-conducting material, electrodes were applied to the pellets prior to poling and piezoelectric measurements. Gold was used as electrode material and was applied by sputtering for 60 seconds. In preparation for the gold-sputtering, the pellets were ground to 1200 grid using SiC-paper. To remove impurities from the grinding process, the pellets were immersed in ethanol in an ultrasonic bath for 10 minutes.

As the material has to be poled in order to show piezoelectric behavior, the pellets were poled in air at an electric field of 700 V/mm for 10 minutes prior to piezoelectric measurements. The poling was conducted using aixACCT TF Analyzer 2000E and TREK 610E as a high voltage amplifier. A current range of 100 μA was used. The set-up used for poling and the piezoelectric measurements is shown in Figure 3.3.1

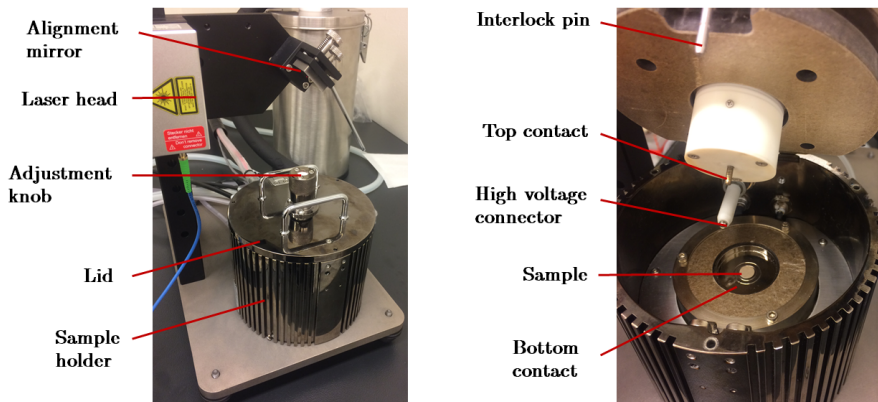


Figure 3.3.1: The figure shows the setup used for the electric poling and piezoelectric measurements.

The piezoelectric coefficient, d_{33} , was measured, by applying a maximum electric field within the range of -700 V to 700 V, using a current range of 1 mA. A small signal frequency of 1 kHz and a small signal amplitude of 10 V was used. 150 data points were measured in each cycle and a long integration time was used. By using a long integration time, the measuring time at each data point is increased (~ 1 s), resulting in a smoother curve.

After the piezoelectric measurements were conducted, the pellets were heated to 140°C for 1 hour to get the ferroelectric domains back to their original randomized state. This was done in order to be able to conduct a second measurement after soaking.

3.3.1 Exposure to saline environment

As the material will be implanted to the body, it is of interest to examine if and how the piezoelectric properties of the material will change after being exposed to a similar environment. The pellets were submersed into a 0.9 % NaCl-solution at 37°C for 14 days.

As the electrode material got damaged during soaking, the electrode layer was removed by grinding the pellets to 1200 grit using SiC-paper. The pellets were submersed in ethanol and cleaned for 10 minutes using an ultrasonic bath in order to remove residual solid particles from the grinding. The pellets were dried at $\sim 100^\circ\text{C}$ for 6 hours, before a new electrode layer was applied by sputtering. The piezoelectric measurements were conducted once more using the same parameters for both poling and the piezoelectric measurements as described in Section 3.3.

3.4 Hardness measurements

To measure the hardness of the material, Vickers' microindentation test was conducted on unpoled pellets. Samples with diameter 15 mm \varnothing were used for this purpose and 0, 20, 40 and 60 vol% added pore former were examined. To minimize the surface roughness, the pellets were ground to 1200 grit, using SiC-paper, prior to the analysis. 5 indentations were made in each sample using a load of 500 g. The reported hardness is the average value of the 5 indentations. On the first 5 measurements of each pellet a load of 1 kg was used, due to broken apparatus.

3.4.1 Exposure to saline environment

After the first hardness test was conducted, the pellets were submersed into a 0.9 % NaCl-solution at 37°C, resembling the environment in the body. The pellets were soaked for 14 days. Every second day, the pellets were taken out and new hardness test were conducted. The pellets were cleaned in ethanol and dried at $\sim 100^\circ\text{C}$ for 30 minutes prior to the measurements.

The first measurement was conducted using DVK-1S Matsuzava, the following four measurements was made using Innovatest Holger X Hartmann and the three final measurements were conducted with LEICA VMHT MOT, as shown in Table 3.4.1. The frequent change of indenter was due to broken apparatus.

Table 3.4.1: Indenter used for the hardness measurements.

Day	Indenter	Load [g]
0	DVK-1S Matsuzava	1000
2-8	Innovatest Holger X Hartmann	500
10-14	LEICA VMHT MOT	500

Chapter 4

Results

4.1 Phase purity

The phase purity of the calcined powder was examined by X-ray diffraction. Six batches of calcined powder were made. The X-ray diffractogram of the second batch of calcined powder is given in Figure 4.1.1. The diffractograms from the remaining batches showed the same reflections, and can be found in Appendix A.

Figure 4.1.1 also includes the diffractogram of a crushed sintered pellet made from the same batch of calcined powder. The diffractograms show the characteristic peaks for tetragonal BaTiO_3 , which are marked with black dots in Figure 4.1.1. The small peaks around 24° and 34° in the diffractogram are due to unreacted BaCO_3 . As these peaks are not present in the diffractogram from the sintered pellet, it is clear that the unreacted precursor powders react during the sintering process. The peaks of the sintered pellet are sharper, as the crystallite size increases during sintering.

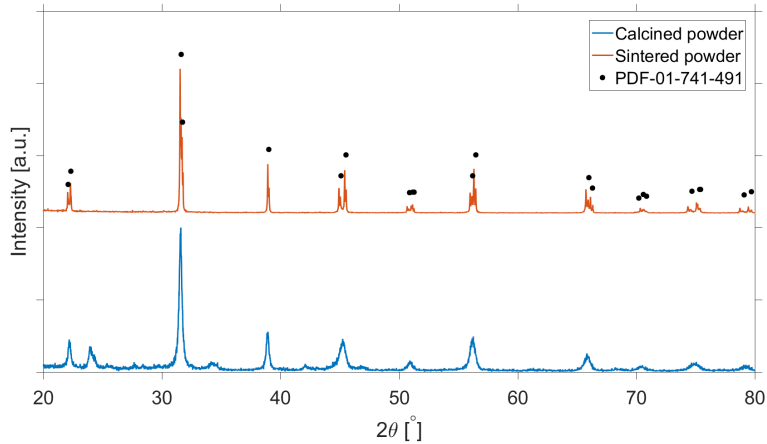


Figure 4.1.1: The diagram compares the XRD diffractogram from calcined powder and powder from a crushed sintered pellet from calcination batch 2. The characteristic peaks of the diffractograms have been fitted with PDF card (01-074-2491) and are marked with black dots.

4.2 Porosity

The relative density of the samples was calculated from values obtained from Archimedes' measurement as well as calculated from weight and size. Figure 4.2.1 shows the values of relative density calculated for the pellets made for the piezoelectric measurement using both methods. It shows that the values obtained from Archimedes' measurement are lower than the values obtained from measuring the dimensions of the pellets. The values shown in the graphs are the average of the 5-6 pellets made for each porosity. The pellets made for the hardness test showed a similar trend. The results from these measurements can be found in Appendix B.

Figure 4.2.2 shows the values obtained from the Archimedes' measurement for the pellets made for the piezoelectric measurement. The pellets made for the hardness test showed similar trends, and can be found in Appendix B. The values

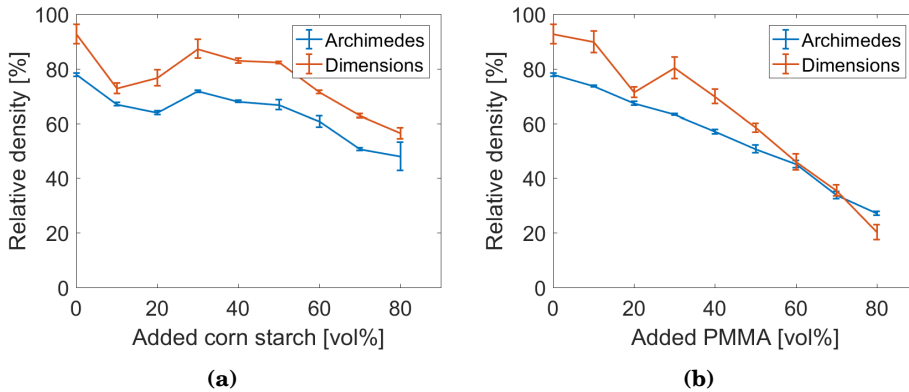


Figure 4.2.1: Figure (a) gives the relative density of the pellets made with corn starch as pore former. Figure (b) gives the relative density of the pellets made with PMMA as pore former. The errorbars give the standard deviation.

of the total, closed and open porosity of all pellets are summed up in Table B.0.1, Appendix B.

Figure 4.2.2 shows that the relative density of the samples decreases linearly with increased amount of pore former added. The deviation from linearity is larger for the samples made with corn starch, suggesting that porosity control is more difficult to achieve when using this pore former. The pellets made with 10 and 20 vol% corn starch had a relative density much lower than expected. As shown in Figure 4.2.2 (a) and (b), the standard deviation of the values are larger for the samples made with corn starch than the samples made with PMMA. Generally, the standard deviation also increases with increasing porosity. A higher total porosity was obtained for the samples where PMMA was used as pore former, as shown in Figure 4.2.2 (b).

As shown in Figure 4.2.2 (c), the porosity was mainly closed. With increasing amount of pore former, the increase in open porosity is larger than the increase in closed porosity, Figure 4.2.2. The standard deviation is generally larger for the open porosity than for the closed porosity.

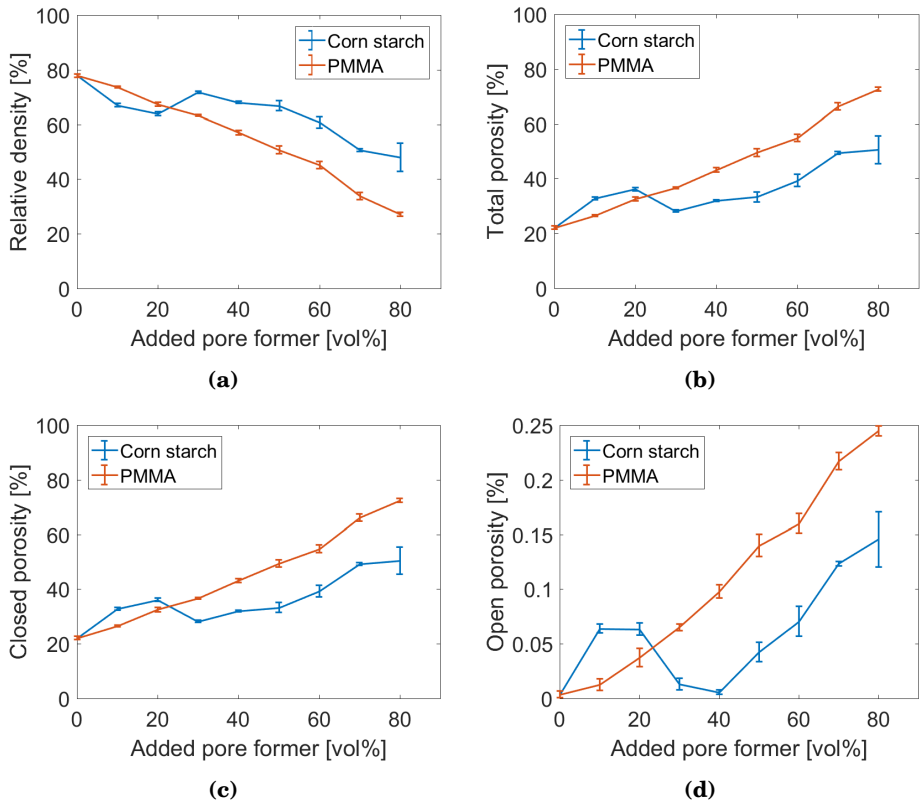


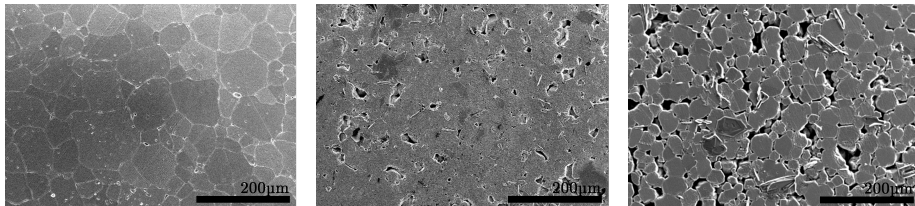
Figure 4.2.2: Figure (a) gives the average relative density of the samples made for the piezoelectric measurements plotted against amount of added pore former. Figure (b) gives the average total porosity of the same samples plotted against the amount of pore former added. Figure (c) and (d) gives the average closed and open porosity, respectively. The errorbars give the standard deviation based on measurements from all pellets of the same porosity.

4.3 Microstructure

The microstructure of the samples was investigated by scanning electron microscopy (SEM) (Hitachi S-3400N).

4.3.1 The effect of calcination temperature

The effect of calcination temperature on the final microstructure was investigated by comparing the microstructure of pellets made from powders calcined at 800, 850 and 900°C. Figure 4.3.1 shows the microstructure of a dense pellet made from each calcination batch.



(a) Calcination temperature 800°C. (b) Calcination temperature 850°C. (c) Calcination temperature 900°C.

Figure 4.3.1: The pictures show the difference in microstructure between pellets made from powder calcined at 800, 850 and 900°C. The SEM images were taken using a magnification of 100x.

The porosity of the dense pellets increased with increasing calcination temperature, as shown in Figure 4.3.1. This is most likely due to coarsening of the particles taking place at higher calcination temperatures. Based on these results, 800°C was chosen as calcination temperature for the following samples.

4.3.2 The effect of mixing

As stated in Section 3.1.2, the PMMA particles formed agglomerates at elevated temperatures during wet mixing. The microstructure of these pellets was investigated using SEM. The agglomerates created craters in the samples, as shown in Figure 4.3.2 (a). However, areas with homogeneous pore distribution were also found in the same pellet, as shown in Figure 4.3.2 (b). Similar inhomogeneous microstructure was observed in pellets of higher porosity. SEM-images of these pellets can be found in Appendix C. Figure 4.3.2 (c) shows the surface of a pellet where PMMA has been added through dry mixing, which resulted in a more homogeneous microstructure.

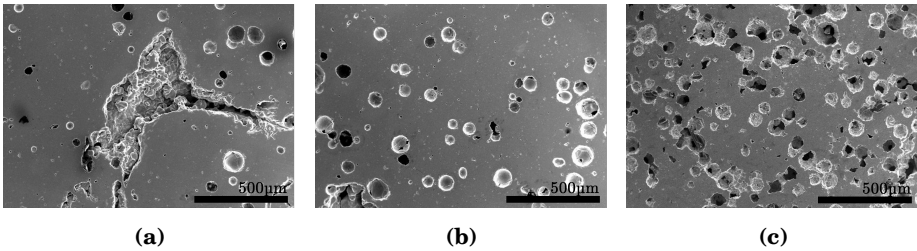


Figure 4.3.2: The pictures show the difference in microstructure between pellets where PMMA had been added through wet mixing ((a) and (b)) and dry mixing (c). Image (a) and (b) shows different areas of the same pellet, made with 20 vol% added PMMA. Image (c) shows the microstructure of a pellet made with 50 vol% added PMMA. The SEM images were taken using a magnification of 100x.

4.3.3 The effect of pore former

Figure 4.3.3 shows SEM-images taken of pellets with 20, 40, 60 and 80 vol% of added pore former of both corn starch and PMMA. The amount of porosity in the pellets increased with the amount of pore former added. The increase in porosity is more evident in the samples made with PMMA, suggesting that a better porosity control is achieved when using this pore former.

The SEM-images given in Figure 4.3.3 show that the pores are homogeneously distributed throughout the material for all porosities and both pore formers, indicating good quality of the mixing routines.

The PMMA resulted in spherical pores of size 50-100 μm , while the corn starch resulted in pores with an irregular shape of size 5-20 μm . The irregular pores showed a higher degree of interconnectivity already for lower porosities compared to the samples with PMMA. The spherical PMMA-induced pores became interconnected the amount of added pore former exceeded 60 vol%, with a pore size of 100-250 μm . The samples made with corn starch formed interconnected pores at lower volume fractions of added pore former (10 vol%). However, the average pore size of the interconnected pores did not reach 100 μm before 80 vol% of pore former was added.

The bright, elongated particles observed in the pellet with 60 vol% added PMMA and the particles found on the sample with 40 vol% added corn starch are most likely due to insufficient cleaning after diamond polishing. The particles were examined using EDS-analysis, which confirmed that the particles mainly consist of carbon.

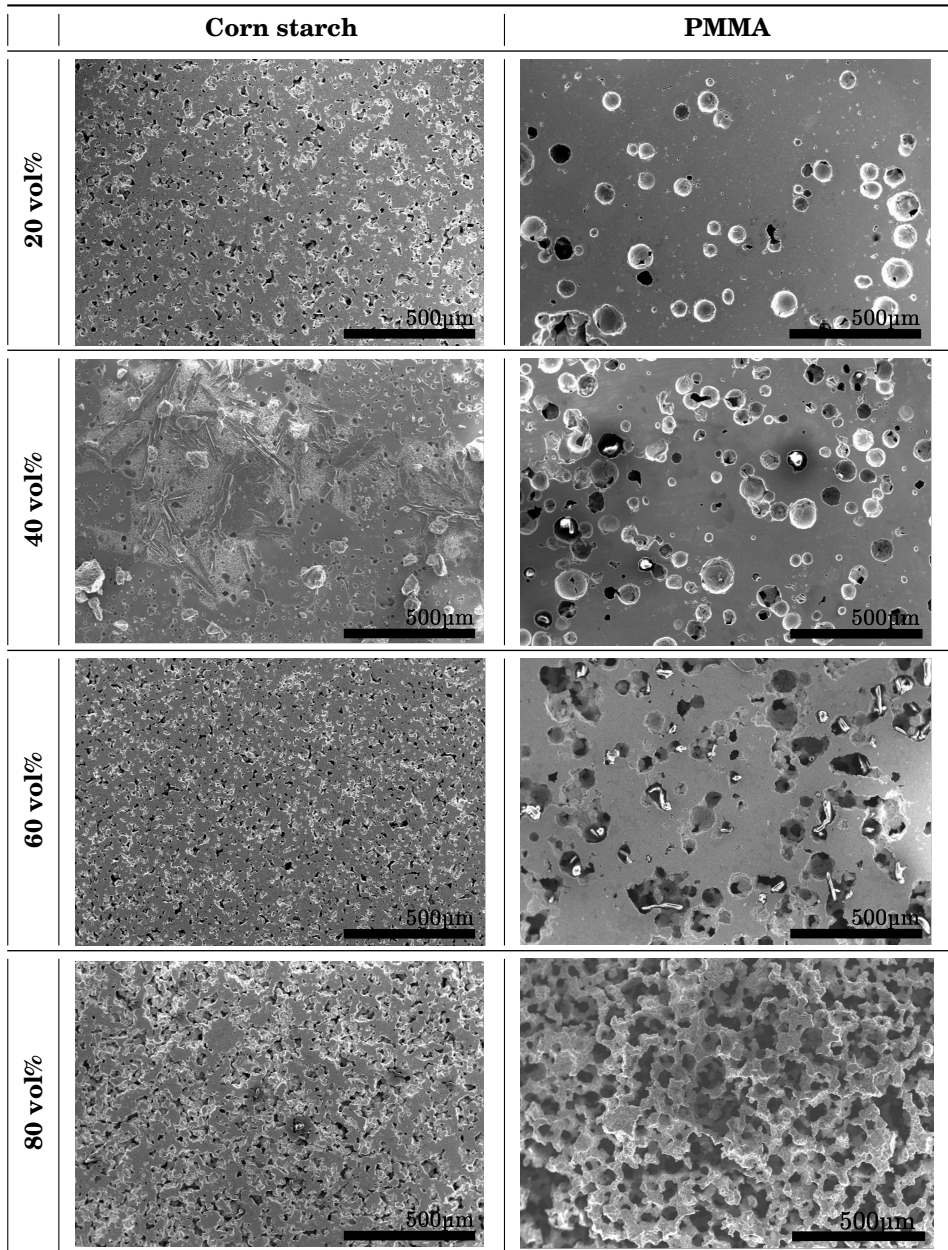


Figure 4.3.3: The figure shows the microstructure of samples made with 20, 40, 60 and 80 vol% corn starch and PMMA. The images were taken using a magnification of 80x.

4.4 Piezoelectric properties

The piezoelectric properties of the pellets were examined by measuring the converse piezoelectric effect before and after soaking in saline solution for 14 days. Pellets made with 70 and 80 vol% PMMA were too fragile to polish, making it impossible to achieve a constant height and apply electrodes. All remaining pellets were successfully poled in air at an electric field of 700 V/mm for 10 minutes prior to the piezoelectric measurement, as described in Section 3.3.

Figure 4.4.2 gives the average remanent piezoelectric coefficient, d_{33}^0 , for all samples. The value is calculated from the absolute value of the positive and negative remanent piezoelectric coefficient found at an electric field of zero, as shown in Figure 4.4.1 The figure includes pellets made with corn starch and PMMA both prior ((a) and (b)) and subsequent to soaking ((c) and (d)).

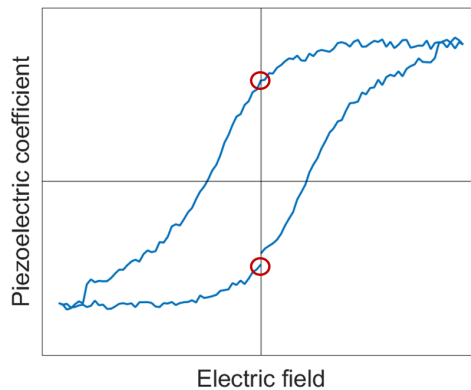


Figure 4.4.1: The figure shows a piezoelectric hysteresis loop for BaTiO_3 . The remanent piezoelectric coefficients are marked with red circles.

Subsequent to soaking, the pellets were polished once more, which lead to decrease in thickness of all pellets. As a result some of the highly porous samples got too thin and fragile and broke, hence there are less data points for the measurements conducted post-soaking.

Figure 4.4.2 clearly shows that there is a decrease in d_{33}^0 when the porosity

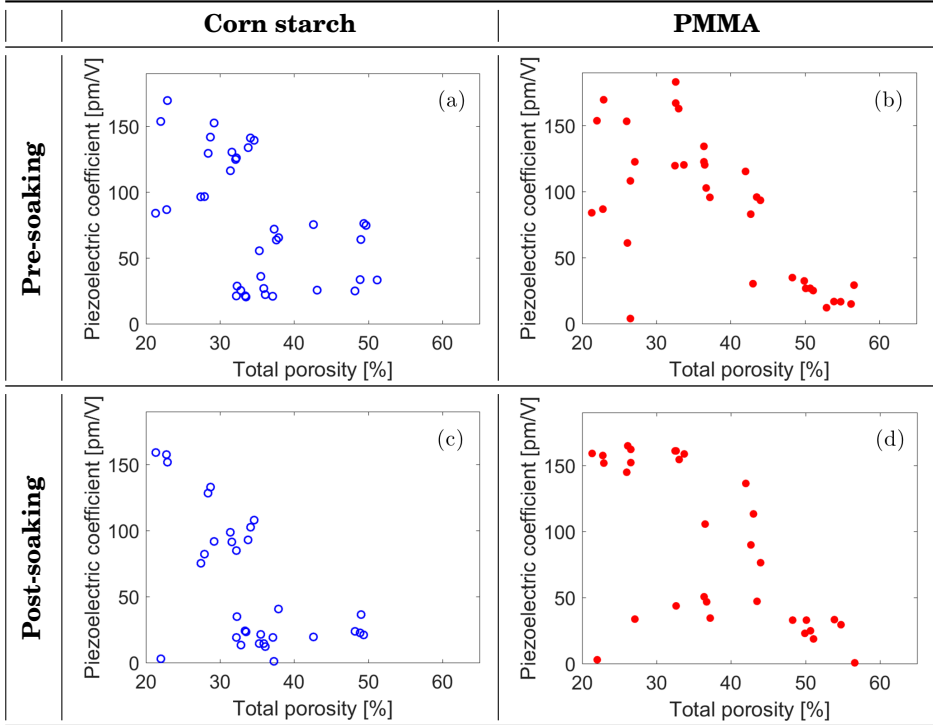


Figure 4.4.2: The figures show the measured values of d_{33}^0 for all pellets plotted against the porosity of each pellet. Figures (a) and (c) show d_{33}^0 for pellets made with corn starch measured prior to soaking and subsequent to soaking. Figure (b) and (d) show the corresponding values of samples made with PMMA.

increases. The decrease is more rapid for the pellets made with corn starch than for the pellets made with PMMA. The values obtained for the pellets made with PMMA are generally higher than the values obtained for pellets made with corn starch.

Large variations in the d_{33}^0 -values are found for most porosities of both pore former. The variation of measured values for d_{33}^0 of the pellets made with PMMA decreased for pellets with 50 and 60 vol% added pore former. These pellets were made through dry mixing, which resulted in a homogeneous pore distribution

(Section 4.3.2). This might be the reason for the decreased spreading of the data points at higher porosities for samples made with PMMA.

Extremely low values observed come from samples that sparked during the measurement. This was only observed in samples with added porosity above 40 vol% for corn starch and 60 vol% for PMMA. The sparking of samples has also contributed to the decreased amount of data points in the measurements conducted subsequent to soaking. Generally, a slight decrease of the d_{33}^0 -values is observed after soaking.

Figure 4.4.3 gives the hysteresis loops of two pellets made with each pore former and compares them to the results for dense pellets. The figure shows the results from the measurement conducted before ((a) and (b)) and after ((c) and (d)) the soaking. The graphs are representative for all pellets made with the same amount of added porosity. Additional graphs can be found in Appendix D. The dense pellet showed a higher d_{33}^0 and a higher $d_{33,max}$ than all porous pellets. The hysteresis loop for the highly porous samples appear elongated with a low d_{33}^0 . The reduced piezoelectric properties in the porous pellets are expected and correspond to results found in literature [10, 38].

The coercive field, E_C changes with changing porosity for the pellets made with corn starch. For the highly porous samples, the hysteresis is asymmetric, with a different E_C for positive and negative bias field.

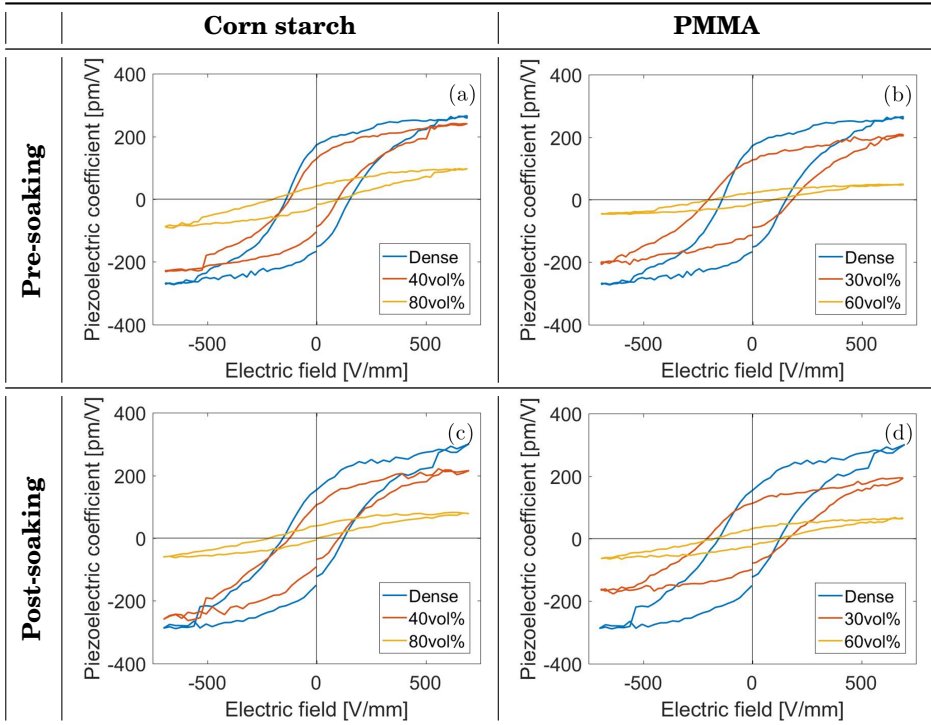


Figure 4.4.3: The figures show the measured values of d_{33} plotted against the porosity of each pellet. Figure (a) and (c) show the hysteresis of samples made with corn starch before and after soaking. Figure (b) and (d) show the corresponding graphs for samples made with PMMA.

4.5 Hardness

The hardness of unpoled pellets of porosities from 0-60 vol% added pore former was examined using Vickers' indentation test. Figure 4.5.1 shows how the hardness of the material changed while being submersed in a saline solution for 14 days. The graphs give the average value of the five indentations conducted on the sample the current day.

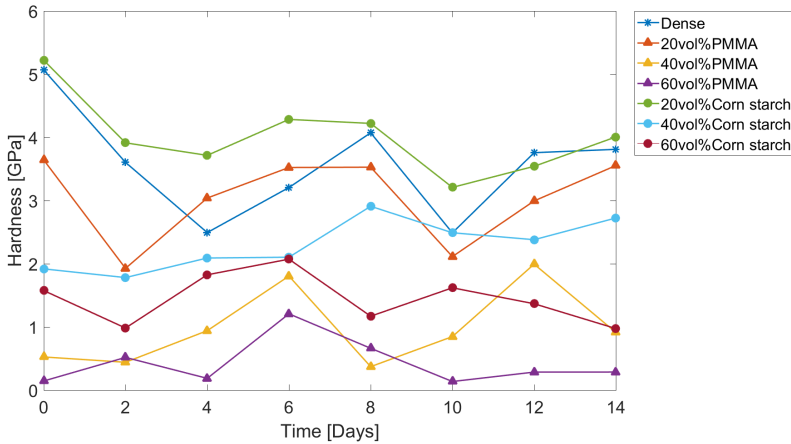


Figure 4.5.1: The figure shows the measured hardness of samples that were submerged in saline solution for 14 days. Measurements were conducted every other day. The values found in the graphs are the average value of five indentations conducted on each sample.

The average hardness of the pellets stayed rather constant during soaking for two weeks. Some variations are seen, but there is no clear trend of increased or decreased mechanical properties. The figure shows that the hardness of the samples decreases with increasing porosity. Pellets where PMMA was used as pore former generally had a lower hardness than samples where corn starch was used as pore former, or it could be a result of the higher porosities achieved when using PMMA. This might be due to the larger size of the pores of the PMMA or the higher final porosity achieved for samples made with PMMA.

The uncertainty of the measurements proved to be extremely large and could not be included in the graph. The uncertainty observed is due to the porous structure of the sample, as a small change in the local microstructure will give a large change in the measured hardness. Even though the pores are homogeneously distributed in the pellets, some variations on the microscale will be present. A table giving the values and standard deviation of the measurements can be found in Appendix E.

Chapter 5

Discussion

5.1 Microstructure

5.1.1 The effect of pore former shape on interconnectivity

As stated in Section 2.3, the pores in a bone implant need to be interconnected with a size $>100\ \mu\text{m}$ in order to allow ingrowth of tissue into the implant. Investigation of the microstructure of the porous samples made, showed that interconnected pores of this size were achieved for pellets made with both pore formers.

For pellets made with corn starch, pores of the desired size were found in pellets with addition of 10 vol% corn starch. These samples exhibited high interconnectivity of the pores even though the pore former content was low. This led to the appearance of some large pores, whereas the average pore size was found to be $\sim 50\ \mu\text{m}$. An average pore size of $100\ \mu\text{m}$ was not observed until addition of 80 vol% corn starch.

The high interconnectivity observed in the samples with 10 and 20 vol% added corn starch compared to the other pellets with the same pore former, could be a result of the different BaCO_3 -precursor powder that was used to make these samples. As listed in Table F.0.1, Appendix F, the BaCO_3 -precursor powder was changed to a more pure powder from batch three.

Pellets with 10 and 20 vol% added corn starch were made using the first precursor powder as well. Due to fracture during sintering, these pellets could not be used for the piezoelectric measurement. Upon SEM-investigation of these pellets, it was revealed that the pores were more separated, as shown in Figure C.0.1. This could be an indication that the precursor powder used could affect the

densification during sintering and hence the final microstructure of the pellets. This could also explain the low density observed for pellets made with 10-20 vol% corn starch used for the piezoelectric measurement, as pointed out in Figure 4.2.2.

Due to the high interconnectivity and low density of the pellets with 10-20 vol% corn starch, there was no significant increase in the amount of interconnected pores between the pellets made with 10-40 vol% added corn starch.

The pores resulting from PMMA particles were within the range of 50-100 μm . However, these pores were separated up to ~ 50 vol% added PMMA. At this volume fraction the particles started to form interconnected pores, within the size range of 100-250 μm . The interconnectivity of the PMMA induced pores grew with increasing amount of added pore former.

The higher interconnectivity observed for the samples made with corn starch is coherent with previous research showing that irregular shaped pore formers result in more interconnected pores than spherical pore formers [10, 38]. This is discussed as a result of the lower aspect ratio of the irregular shaped pores, which will increase the occurrence of interconnectivity in these samples [10]. It is also suggested that the interconnectivity is related to the decomposition rate of the pore formers [38]. Wang *et al.* (2008) stated that a slow decomposition rate would lead to higher interconnectivity of the samples. In their experiment, the burn off and sintering was conducted in one step, resulting in decomposition of pore former and densification occurring at the same time. As the sintering and burn off occurs in two different steps in the current study, the decomposition rate should not affect the densification. The high interconnectivity of the samples made with irregular shaped pores, is therefore believed to be a result of the aspect ratio of the pores.

5.1.2 The effect of pore size and shape on shrinkage during sintering

The results given in Section 4.2 and 4.3 clearly show that a better porosity control was achieved for samples made with PMMA than for samples where corn starch was used as pore former. Samples made using corn starch as a pore former had significantly lower final porosity than what was added. A decrease in porosity is expected, as shrinkage will occur during sintering. However, the difference between the final porosity of the pellets made with PMMA and corn starch is significant. This suggests that shrinkage is dependent on either pore size or shape, as the PMMA particles are both larger and more spherical than corn starch. Experiments examining pore formers of different shape generally show that an irregular shape leads to more shrinkage than a spherical shape [39]. Zhang *et al.* (2007) [10] suggests that all pores decrease with the same rate in all directions. This will result in closing of the irregular shaped pores due to shrinkage in the directions where the diameter of the pores is small, as shown in Figure 5.1.1. According to Zhang, the rate of shrinkage is also the reason for closing of the smallest pores, with both irregular and spherical shape. This would also lower the final porosity of the samples. It is therefore believed that more of the corn starch induced pores disappeared during sintering, as they are both smaller and less spherical than the PMMA induced pores, resulting in a lower final porosity.

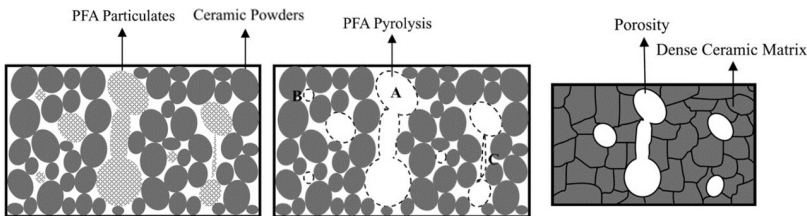


Figure 5.1.1: The schematic illustrates the shrinkage of pore former induced porosity of ceramics. Figure (a) represents the compact green body prior to burn off and sintering. Figure (b) shows the same area after burn off of the pore former. Figure (c) shows the final microstructure of the porous ceramic. Pores marked with B disappears during sintering, while larger pores (A) remain. Figure adapted from Zhang *et al.* (2007) [10].

5.1.3 The effect of mixing procedure

A homogeneous pore distribution was achieved for both pore formers, after optimizing the mixing procedure. As addressed in Section 4.3.2, the PMMA particles agglomerated upon wet mixing with ethanol at elevated temperatures. This led to a final microstructure with an inhomogeneous pore distribution. Previous experiments conducted on porous ceramics using the sacrificial template method with PMMA as pore former showed successfully mixing of PMMA and precursor powder using ethanol as solvent [39]. It is therefore believed that the elevated temperature caused the agglomeration, even though the melting point of PMMA is 105°C, which is 35°C higher than the temperature used for the evaporation of ethanol [52]. Mixing with ethanol will thus demand lower temperature, leading to longer time for evaporating the solvent. As the PMMA and precursor powders were successfully dry mixed manually, this is suggested as a more efficient mixing procedure.

The wet mixing of precursor powder and corn starch using the ultrasonic bath, then a magnetic stirrer and hot plate, was mostly successful. However, previous work on porous barium titanate with corn starch as pore former showed that a better porosity control was achieved upon wet mixing only using the ultrasonic bath [1]. Due to the size of the batch, it was not possible to achieve a good mixture using this method, hence, the additional mixing step using a magnetic stirrer was added to the processing route.

5.2 Electric poling and piezoelectric properties

The dense pellets displayed good piezoelectric properties after poling, as shown in Figure 4.4.3. With increasing porosities the hysteresis loop changed and became more elongated and compressed. As pointed out in Section 4.4, the hysteresis loops of the highly porous pellets were more asymmetric, with a greater change in E_c for the positive and negative bias field. This is possibly due to the varying microstructure of the different pellets, with larger variations for the highly porous pellets.

5.2.1 The effect of pore former and amount

As shown in Figure 4.4.2, the samples made with PMMA exhibited better piezoelectric properties. The samples made with corn starch showed a sudden decrease in d_{33}^0 at porosities around 35 vol%. As for samples made with PMMA, the decrease was more linear, with a slightly more sudden decrease around 50 vol%.

These results are coherent with previous research, showing that samples containing spherical pores have better piezoelectric properties than samples with irregular shaped pores of the same porosity [10, 39]. The reason for this is discussed to be the local electric field enhancement found in the area around a pore (Figure 2.5.1) [48]. This effect leads to incomplete poling of the samples, which will decrease the piezoelectric properties. As addressed in Section 2.2, a spherical pore would lead to a lower electric field enhancement than what would occur around an irregular shaped pore, resulting in better piezoelectric properties for the samples made with spherical pore formers.

The large variations observed for the d_{33}^0 -values obtained for the samples made with PMMA for porosities below 50 vol% (Figure 4.4.2) is most likely due to the inhomogeneous microstructure arising from wet mixing. Even though the pellets made with the same amount of pore former had the same final density, there were large variations in the microstructure, due to agglomeration of the PMMA-particles, as shown in Section 4.3.2. As the poling behaviour strongly depends on the microstructure of the samples, this could be the reason for the varying piezoelectric properties obtained for pellets with <50 vol% added PMMA.

Large variations in the d_{33}^0 -values obtained for the corn starch samples were also observed. These variations were not found within a batch with the same amount of added pore former, but between batches where different amount of pore former was added, but the same final density was achieved. This is a result of the previously discussed densification mechanism occurring during sintering (Section 5.1.2). However, as the irregular pores are oriented rather randomly, a bit of variation in the properties could be expected, as the electric field distribution will be unique in each sample.

5.2.2 The effect of soaking

A significant decrease in the measured piezoelectric properties of the pellets was observed after soaking for 14 days, as shown in Figure 5.2.1. The figure gives the average d_{33}^0 of all pellets made with the same amount of pore former. These results are inconsistent with results from previous research on the BaTiO_3 . Yu *et al.* (2011) observed little change of the piezoelectric properties of BaTiO_3 after being soaked in saline solution for up to 28 days [41]. However, their study was conducted on dense BaTiO_3 ceramics.

Porous samples, as used in the present study, have a larger surface area exposed to the saline solution, which means a larger area for reaction or decomposition to occur. However, optical inspection of the samples showed no sign of decomposition or swelling, which is consistent with previous results [33, 41]. If this was the case, the decrease in properties should be more pronounced for higher porosities. Figure 5.2.1 shows that the samples with initially higher d_{33}^0 , faced a stronger reduction than sample with an initially lower d_{33}^0 .

It was observed that the decrease in piezoelectric properties was more evident for samples with similar porosity, but large d_{33}^0 -values. As no mechanical deterioration or swelling of the samples was observed, it suggests that electrical poling procedure after soaking could not induce the same poling state as before soaking. The influence of poling depends significantly on the quality of the electrode-sample contact and with this on the microstructure present at the sample surface. Since the samples were re-polished and new electrode material was applied, the contact area and quality of the electrode might be altered, leading to changes of the poling state and the obtainable piezoelectric coefficient.

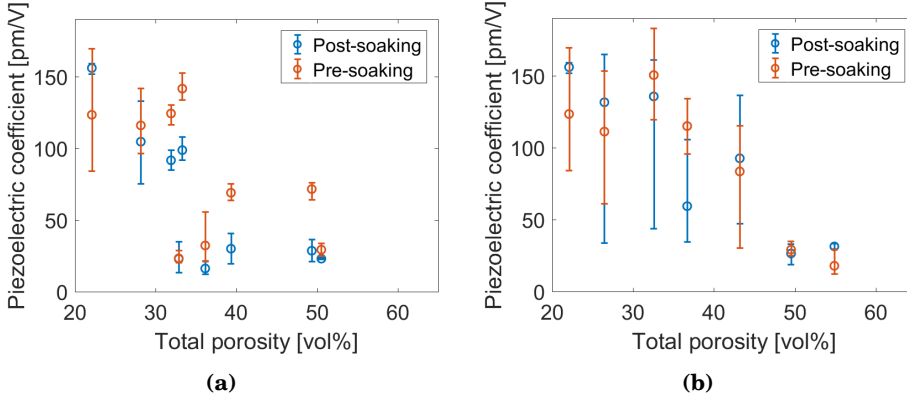


Figure 5.2.1: Figure (a) shows the average d_{33}^0 value for each porosity of the samples made with corn starch prior and subsequent to soaking in saline solution. Figure (b) shows the average d_{33}^0 value for each porosity of samples made with PMMA, before and after soaking in saline solution. The error bars in both figures give the maximum and minimum d_{33}^0 value measured for each porosity.

5.3 Mechanical properties

The hardness test was conducted in order to examine if the introduction of controlled porosity would affect the brittleness of the material. As addressed in Section 4.5, a large uncertainty was observed in the hardness test results. The Vickers' microindentation measurement measures the microstructure of the exact area where the indent is made. Even though the microstructure of the pellets was homogeneous, there were small differences in the microstructure of each area. These differences resulted in large variations of the results.

Some measurements were conducted on an area that appeared dense, but with a pore beneath the surface layer. These measurements resulted in fracture of the thin layer of material between the pore and the indenter. These measurement did not only result in an extremely low hardness, it also lead to difficulties reading off the results. In some of these cases the corners of the indent were

placed in a pore, which made it impossible to give an accurate result. This is demonstrated in Figure 5.3.1, where the indent in a dense area is shown (a) and the indent in a porous area is shown (b).

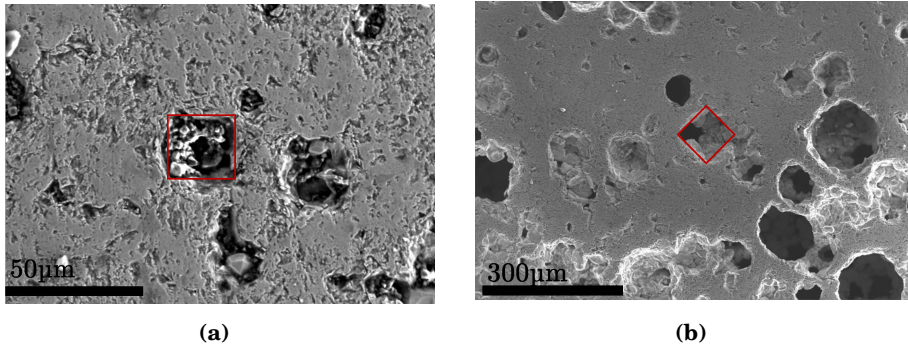


Figure 5.3.1: Image (a) shows an indent made in a pellet with 20 vol% added corn starch. A magnification of 800x was used. Image (b) shows a larger indent, made in a pellet with 40vol% added PMMA. The image is taken with a magnification of 150x. The indents are marked with red squares.

As it turned out to be difficult to measure the bulk hardness of the samples, it is suggested to rather use a test that measures the global mechanical properties of the bulk material, such as a compression test.

5.3.1 The effect of pore former and amount

As addressed in Section 2.1, the amount of porosity, pore size and shape have proven to have an effect on the mechanical properties of a ceramic material. Despite the uncertainty of the measurement, some general trends were observed. As the hardness of bone is within the range of 0.23-0.76 GPa (Table 2.1.1, Section 2.1.2), it is desired that the hardness of the samples are within or slightly above this range. This was only obtained for the samples with 40-60 vol% added corn starch and 40 vol% PMMA. However, as the uncertainty was large, other porosities could face the requirements.

Little research has been conducted on the hardness of porous piezoelectric ce-

ramics, hence there are few results to compare the observations to directly. However, mechanical properties, such as compressive strength and fracture toughness, dependency on porosity is well investigated, showing that mechanical properties generally decrease with increased porosity, as it introduces higher stress concentrations in the material [11].

There is a linear relation between the microhardness and the compressive strength of a material (Equation 2.1.2 and 2.1.3, Section 2.1). Previous experiments measuring the compression strength of porous BaTiO₃ based ceramics have shown to decrease upon increased porosity [17, 53]. This gives an indication of the general trends, but no conclusions can be drawn this comparison.

In addition to decreasing hardness with increasing porosity, it was observed that the pellets made with PMMA had a lower hardness than pellets made with corn starch with the same added porosity. This is inconsistent with the principle addressed in Section 2.1.1, stating that irregular shaped pores introduces more stress in the material than spherical pores, and hence decreases the mechanical properties [11]. As previously discussed, the samples made with PMMA resulted in a higher final porosity than samples made with similar volume fraction of added corn starch, which could be the reason for the lower hardness. Another reason for the lower properties of the pellets with PMMA-derived pores could be the size of them. The mechanical properties of a ceramic decreases with increased pore size [11]. The large pores of the PMMA could also lead to larger indents if the indent was made on top of a pore. This would lead to a great decrease of the average hardness measured for the pellet.

Chapter 6

Conclusion

Porous samples of BaTiO₃ were successfully made with porosity within the range of 20-60 vol%, using corn starch and PMMA as pore formers. The samples made with PMMA resulted in spherical pores, while the samples made with corn starch resulted in irregular shaped pores. A higher porosity was achieved for samples using PMMA, as the driving force for shrinkage is larger for irregular shaped pores than for spherical pores.

A final pore size of 50-100 μm was achieved for the samples made with PMMA. At porosities above 50 vol% added PMMA, interconnected pores of size 100-250 μm were formed. The samples made with corn starch resulted in irregular shaped pores of size 5-20 μm, which formed interconnected pores already at 10 vol% added corn starch. The size of the interconnected pores increased with the amount of added pore former and the maximum size of the interconnected pores made with corn starch was 100 μm, obtained when 80 vol% corn starch was added.

All pellets were successfully poled at an electric field of 700 V/mm, except for the pellets made with 70-80 vol% PMMA, as these were too fragile to conduct the measurements on. A maximum d_{33}^0 of 169 pm/V was measured for the dense samples. The piezoelectric properties of the porous samples decreased with increasing porosity, due to local electric field enhancement in the areas surrounding a pore. As the field enhancement is larger around irregular shaped pores, the decrease in d_{33}^0 was more sudden for the samples made with corn starch than samples made with PMMA. For the samples with a final porosity >45 vol%, the remanent piezoelectric coefficient was ~45 pm/V. A decrease of the piezoelectric

properties after soaking in saline solution for 14 days was observed. As there were no signs of decomposition of the pellets after soaking, the decreased piezoelectric properties are believed to be a result of altered microstructure of the pellet surface after soaking and re-polishing. This would change the quality of the pellet-electrode interface, and hence, change the poling and piezoelectric properties.

The hardness of the pellets decreased with increasing porosity, due to increased stress concentration in the samples. Pellets made with PMMA displayed a lower hardness than pellets made with corn starch. This is discussed to be due to the large size of the pores, which decreases the mechanical properties. The hardness of the pellets remained rather constant during soaking in saline solution for 14 days. Large uncertainties were observed in the results of the hardness measurements, due to local variation of the microstructure.

When comparing the results obtained for the two pore formers, it was observed that the use of PMMA as pore former is favourable, as it results in better porosity control and better piezoelectric properties. Interconnected pores of the wanted size ($>100\ \mu\text{m}$) were achieved at a volume fraction of 50 vol% added pore former, which is lower than for samples made with corn starch. Even though the value of the piezoelectric coefficient obtained for this porosity ($\sim 45\ \text{pm/V}$) is low compared to dense BaTiO_3 , it is higher than the value for bone ($1\ \text{pm/V}$). At this porosity, there is little decrease in the piezoelectric properties after soaking, which is promising.

The mechanical properties were significantly better for the samples made with corn starch. However, as the method for hardness testing was inaccurate, other mechanical tests, such as compression testing or nanoindentation, should be conducted before excluding the use of PMMA as pore former in porous BaTiO_3 for the use of bone implant.

Chapter 7

Further work

As the hardness test showed large uncertainties, it is suggested to conduct a compression test in order to investigate the compression strength of the bulk material or nanoindentation to examine the properties on a microscale. This will give more knowledge on how the mechanical properties of the material changes upon increased porosity and will also allow investigation of the effect of pore size shape. The mechanical tests should also be conducted on poled samples, as poling affects the fracture toughness of a ferroelectric material.

Further work could also include a biocompatibility test, where the material is submersed in a cell culture, to examine if any reactions occur.

Other ways of making porous structures with more open and interconnected porosity could be investigated, such as the replica technique or direct foaming method. The use of coatings on existing implants to make them more functional are in the scope of future work as well.

Appendix A

Additional X-ray diffractograms

X-ray diffraction was used to investigate the phase purity of the calcined powder. The results from every batch made are given in Figure A.0.1. Diffractograms from a crushed sintered pellet from batch 2 is given in Section 4.1.

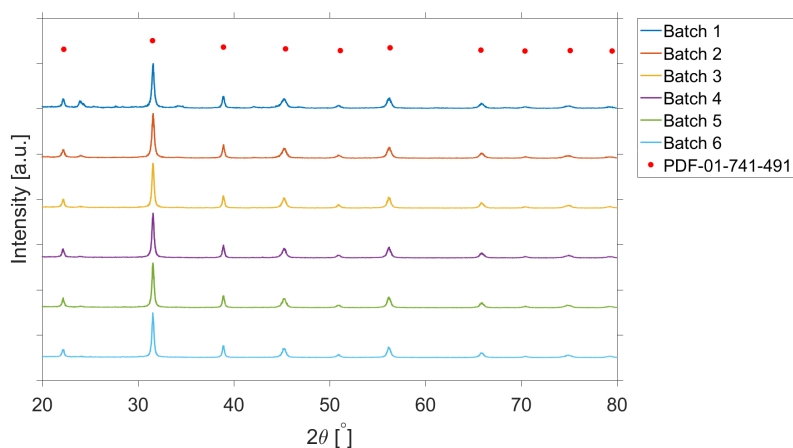


Figure A.0.1: XRD diffractograms from all calcined batches. The characteristic peaks for BaTiO_3 are marked with red dots. The diffractograms were fitted to the PDF card 01-074-2491 using Diffrac.EVA V4.2 software.

Appendix B

Density plots

The relative density and total porosity of the pellets made for the hardness test is presented in Figure B.0.1. The values were obtained using Archimedes' measurement. Two samples of each porosity was made. The values plotted in Figure B.0.1 shows the average value of two pellets.

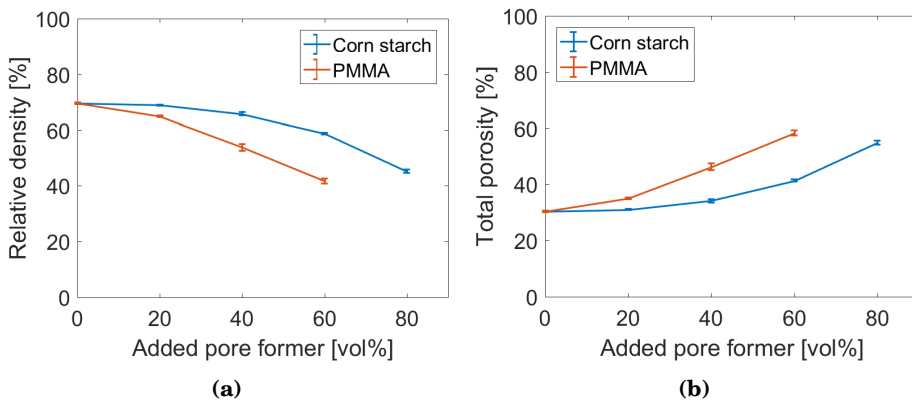


Figure B.0.1: Figure (a) gives the average relative density of the samples made for the mechanical measurements plotted against amount of added pore former. Figure (b) gives the average total porosity of the same samples plotted against the amount of pore former added. The errorbars gives the standard deviation.

Figure B.0.2 shows the closed (a) and open (b) porosity of the samples made for the hardness test plotted against amount of added pore former. The values represented were obtained using Archimedes' measurement and gives the aver-

age of the two pellets made for each porosity.

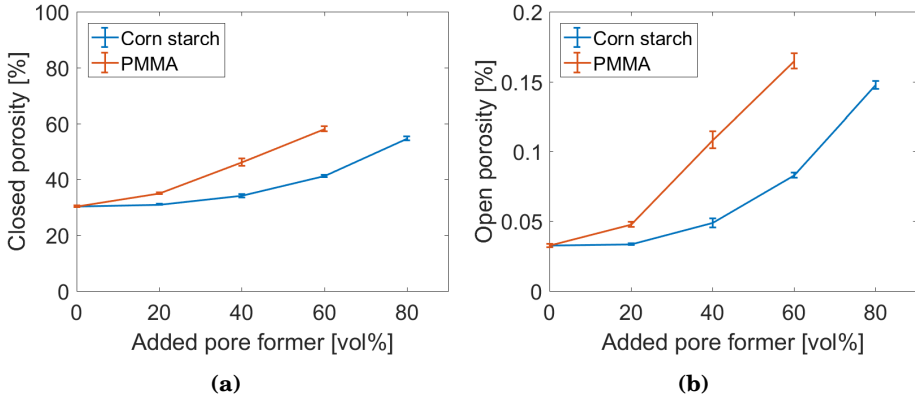


Figure B.0.2: Figure (a) gives the average closed porosity of the samples made for the piezoelectric measurements plotted against amount of added pore former. Figure (b) gives the average open porosity of the same samples plotted against the amount of pore former added. The errorbars gives the standard deviation.

The value of the total, open and closed porosity plotted in the graph can be found in Table B.0.1. Table B.0.2 gives the corresponding values for the pellets made for the piezomeasurement. The graphs showing these values can be found in Section 4.2.

Table B.0.1: The results from the Archimedes' measurement of the pellets made for the hardness tests. The table includes total, closed and open porosity.

Added porosity	Total porosity [%]	Closed porosity [%]	Open porosity [%]
-	30.30	30.27	0.03
20vol% Corn starch	31.02	30.98	0.03
40vol% Corn starch	34.19	34.14	0.05
60vol% Corn starch	41.30	41.21	0.08
80vol% Corn starch	54.81	54.66	0.15
20vol% PMMA	34.97	34.92	0.05
40vol% PMMA	46.22	46.11	0.11
60vol% PMMA	58.26	58.09	0.16

Table B.0.2: The results from the Archimedes' measurement of the pellets made for the piezoelectric measurements. The table includes total, closed and open porosity.

Added porosity	Total porosity [%]	Closed porosity [%]	Open porosity [%]
-	22.09	22.09	0.00
10vol% Corn starch	32.86	32.79	0.06
20vol% Corn starch	36.14	36.08	0.06
30vol% Corn starch	28.19	28.18	0.01
40vol% Corn starch	31.90	31.89	0.01
50vol% Corn starch	33.30	33.26	0.04
60vol% Corn starch	39.33	39.26	0.07
70vol% Corn starch	49.34	39.26	0.12
80vol% Corn starch	50.53	50.38	0.15
10vol% PMMA	26.46	26.45	0.01
20vol% PMMA	32.56	32.53	0.04
30vol% PMMA	36.69	36.62	0.07
40vol% PMMA	43.19	43.09	0.10
50vol% PMMA	49.53	49.39	0.14
60vol% PMMA	54.88	54.72	0.16
70vol% PMMA	66.43	66.21	0.22
80vol% PMMA	72.66	72.42	0.25

Appendix C

Additional SEM-images

Figure C.0.1 compares the microstructure of two pellets made with 10 vol% added corn starch, using different precursor powders. Figure C.0.1 (a) was made with the same precursor powder as the rest of the pellets made with corn starch for the piezoelectric measurement. Figure C.0.1 was made with the same precursor powder as the pellets made with PMMA as pore former.

SEM-images showing the microstructure of pellets made with 10-80 vol% using corn starch and PMMA as pore formers, can be found in Figure C.0.2.

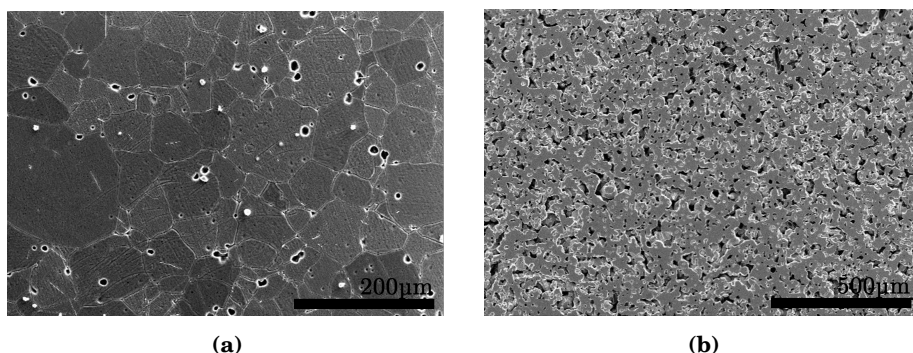
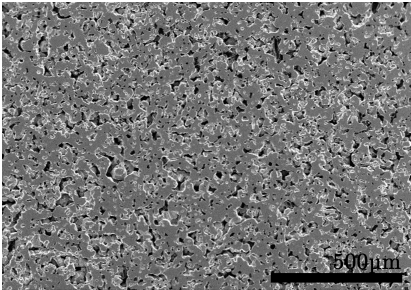
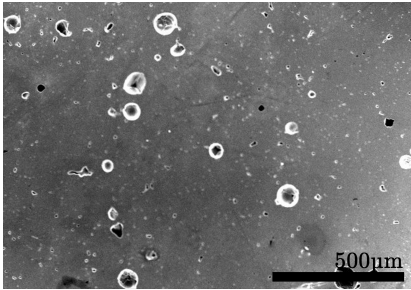
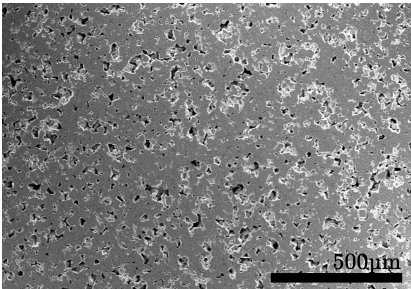
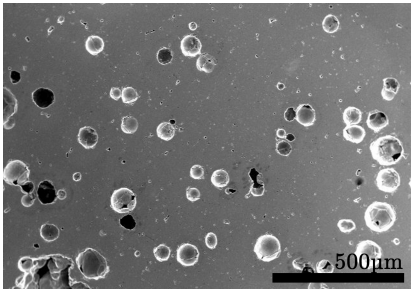
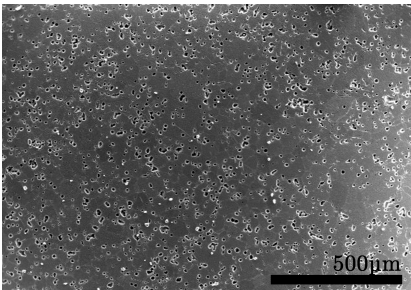
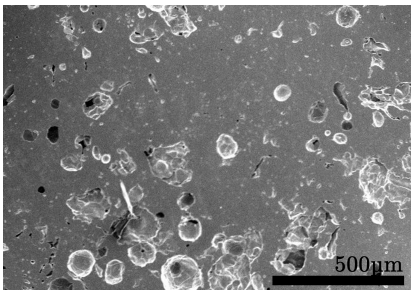
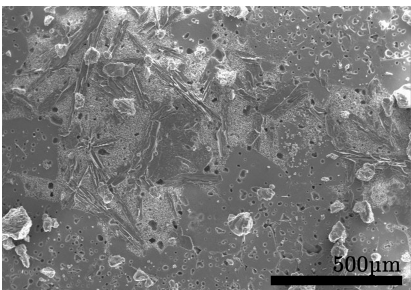
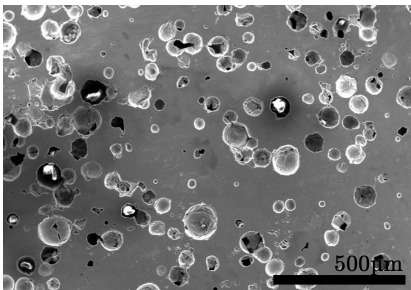


Figure C.0.1: Both figures show the microstructure of pellets made with 10 vol% added corn starch. Figure (a) shows a pellet made with BaCO_3 -precursor powder with >99% purity, while figure (b) shows a pellet made with BaCO_3 -precursor with 99.98% purity. Figure (a) was taken with a magnification of 100x, while figure (b) was taken with a magnification of 80x.

	Corn starch	PMMA
10 vol%		
20 vol%		
30 vol%		
40 vol%		

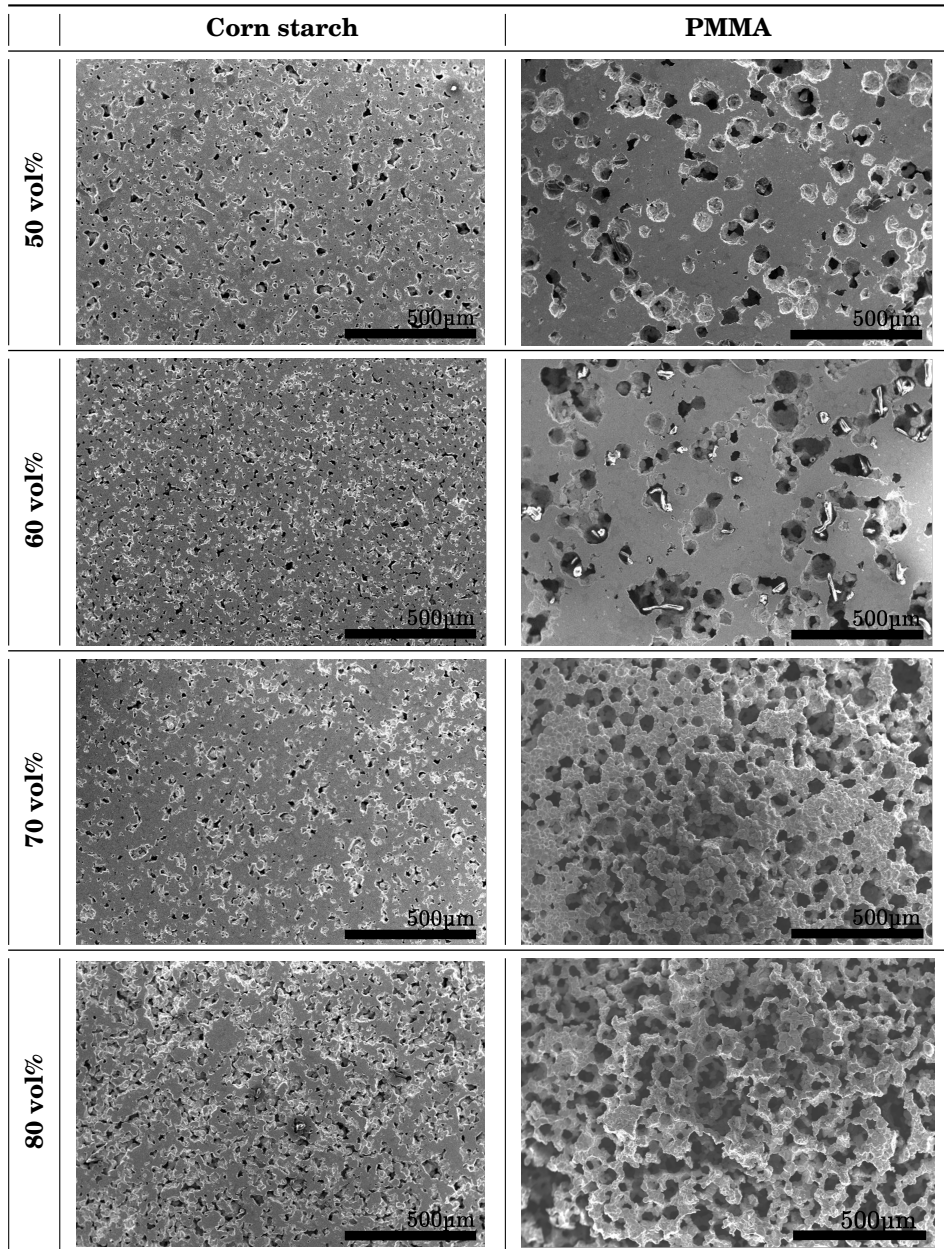


Figure C.0.2: The figure shows the microstructure of samples made with 10-80 vol% added corn starch and PMMA. The images were taken with a magnification of 80x.

Appendix D

Additional hysteresis loops

Figure D.0.1 shows the hysteresis loops a dense pellet measured before and after soaking. The hysteresis loops for the porous pellets before and after soaking can be found in Figure D.0.2. These loops are representative for most pellets made with the same amount of added porosity.

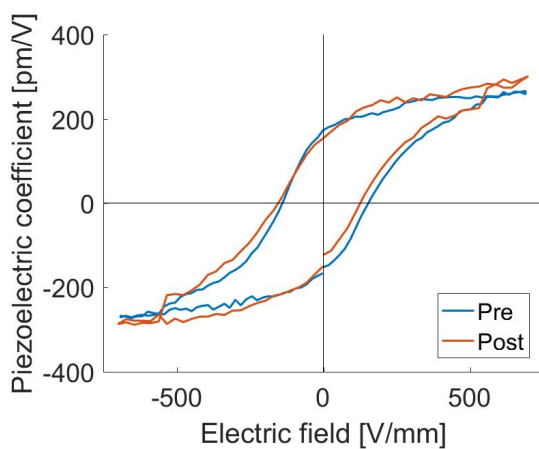
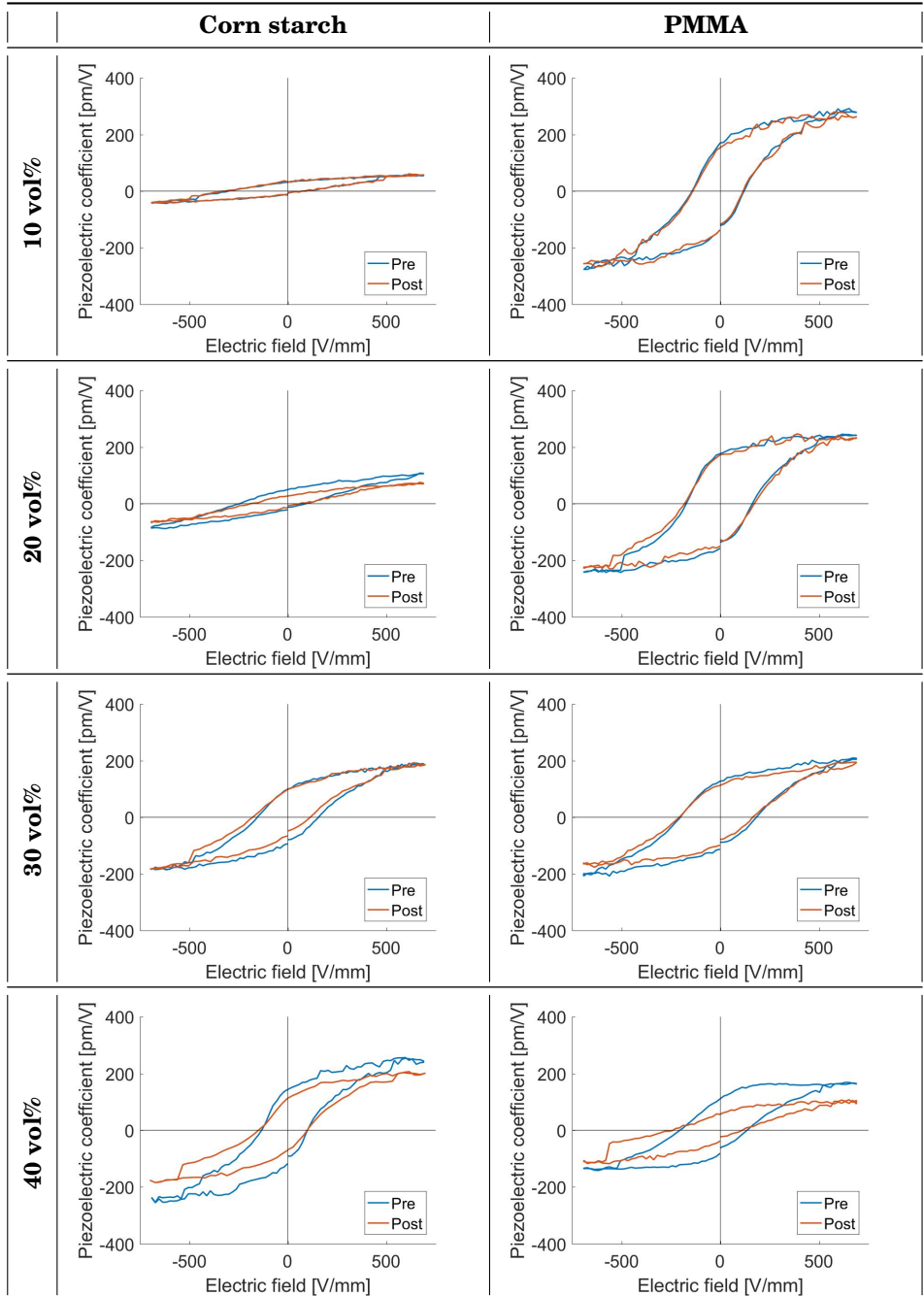


Figure D.0.1: The figure shows the hysteresis loops of a dense pellet measured before and after soaking.



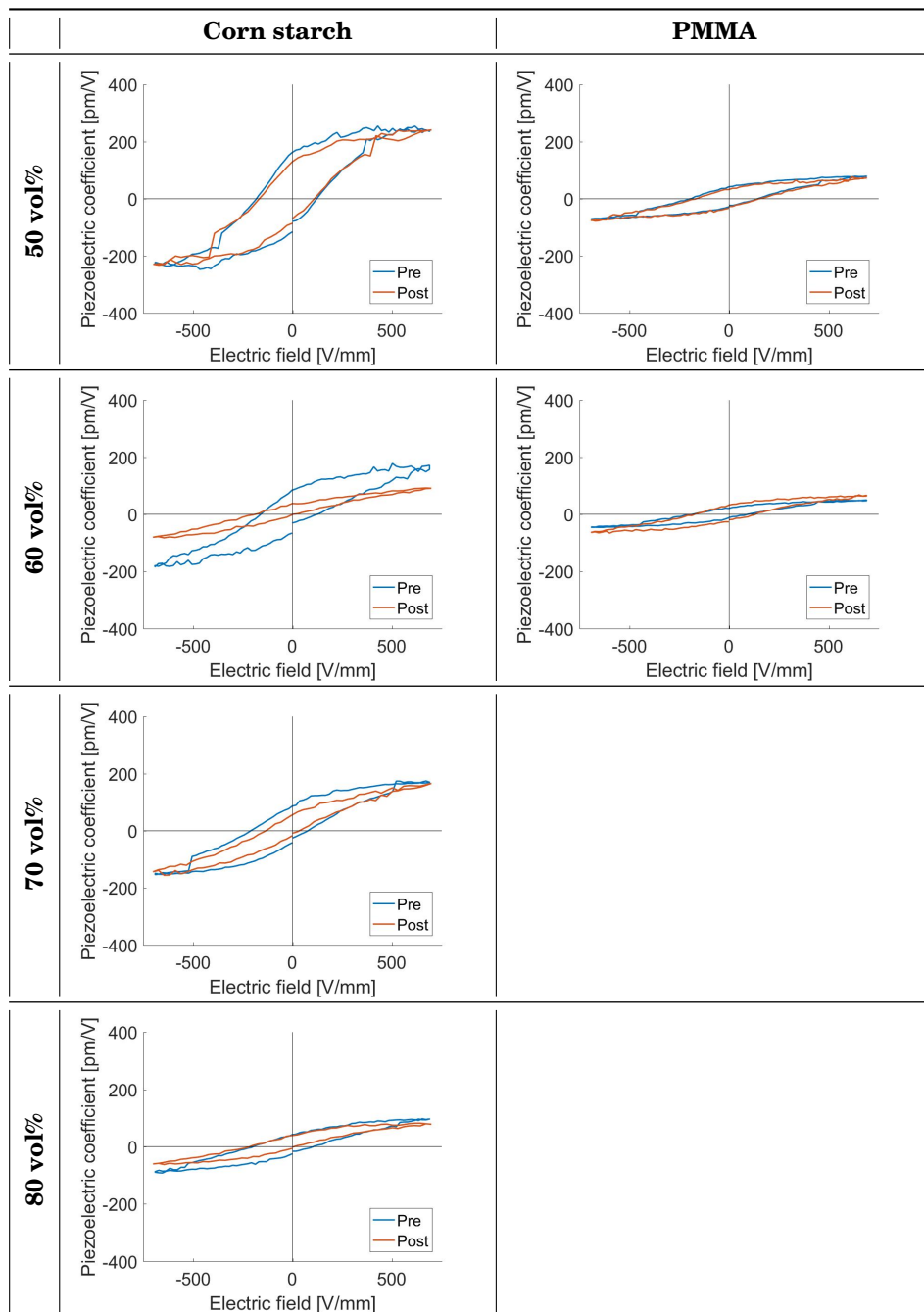


Figure D.0.2

Appendix E

Table mechanical testing

Table giving values for all hardness measurements conducted, including standard deviation of the average value for each pellet each day can be found in Table E.0.1.

Table E.0.1: The values of the hardness tests conducted, including average values for each day (AVG) and the standard deviation (STDEV).

#	Indent	Day 0	Day 2	Day 4	Day 6	Day 8	Day 10	Day 12	Day 14
124	1	516.0	71.9	390.6	503.8	351.6	340.0	499.0	38.0
	2	387.8	79.0	78.6	140.5	125.6	17.4	433.0	473
	3	143.4	29.6	370.6	260.1	570.9	287.0	483.0	446.0
	4	407.6	387.7	373.8	506.0	375.7	350.0	56.9	424
	5	401.6	414.5	336.4	386.2	375.2	83.3	54.9	431
	AVG	371.3	196.5	310.0	359.3	359.8	215.5	305.4	362.4
	STDEV	122.8	168.1	117.0	142.0	141.4	138.2	204.8	163.1
127	1	53.2	18.7	86.9	41.5	36.3	352.0	150.0	33.2
	2	56.0	33.9	150.2	300.9	26.5	18.7	157.0	39.6
	3	69.3	75.4	74.4	71.2	31.9	10.0	309.0	276.0
	4	28.1	29.7	141.0	185.9	44.81	11.6	381.0	64.3
	5	61.3	67.4	27.4	321.1	50.2	40.0	19.7	52.9
	AVG	53.64	45.0	96.0	184.1	37.9	86.4	203.3	93.2
	STDEV	13.9	22.2	45.2	114.5	8.6	133.2	127.6	92.0

#	Indent	Day 0	Day 2	Day 4	Day 6	Day 8	Day 10	Day 12	Day 14
128	1	20.7	2.2	31.2	12.4	7.5	5.1	12.5	48.2
	2	8.4	23.5	26.3	110.0	70.0	25.0	12.5	16.3
	3	22.0	15.0	14.4	440.0	45.8	9.4	48.4	8.15
	4	16.0	103.4	17.8	9.9	91.7	16.9	16.1	65.1
	5	7.2	120.3	5.7	43.7	111.9	13.5	56.3	8.5
	AVG	14.9	52.9	19.1	123.2	65.6	14.0	29.6	29.3
	STDEV	6.1	48.9	9.0	162.5	35.4	6.8	19.1	23.2
131	1	374.7	257.4	350.8	312.4	514.1	239.0	408.0	403.0
	2	481.6	359.4	270.9	316.4	422.7	211.0	370.0	285.0
	3	541.9	410.2	195.8	240.3	360.2	368.0	314.0	362.0
	4	495.9	369.7	322.2	381.8	484.0	376.0	316.0	560.0
	5	688.4	441.2	131.8	384.2	295.4	75.3	508.0	333.0
	AVG	516.5	367.6	254.3	327.0	415.3	253.9	383.2	388.6
	STDEV	101.9	62.4	80.8	53.1	80.0	111.3	71.7	93.9
132	1	486.3	457.8	309.6	398.2	324.5	362.0	426.0	373.0
	2	872.6	409.1	366.9	382.8	590.7	325.0	429.0	459.0
	3	391.2	318.2	404.4	517.1	475.2	245.0	436.0	393.0
	4	385.6	400.2	360.7	421.6	408.1	389.0	256.0	440.0
	5	525.6	410.2	452.8	464.8	353.7	315.0	259.0	378.0
	AVG	532.3	399.1	378.9	436.9	430.4	327.2	361.2	408.6
	STDEV	178.6	45.2	47.7	48.7	95.2	48.9	84.7	34.6
135	1	140.3	169.1	385.2	158.2	310.6	149.0	201.0	210.0
	2	147.3	335.6	119.2	113.2	186.3	363.0	237.0	355.0
	3	322.8	218.4	157.2	245.4	199.6	274.0	205.0	264.0
	4	215.8	85.82	253.1	307.9	430.7	291.0	445.0	210.0
	5	152.4	99.48	151.4	248.1	356.3	193	126.0	350.0
	AVG	195.7	181.68	213.2	214.6	296.7	254.0	242.8	277.8
	STDEV	69.0	90.7	96.9	69.6	93.1	75.3	107.5	64.1
137	1	103.8	124.8	402.3	92.34	186.2	196.0	425.0	46.0
	2	331.9	34.6	88.5	28.4	62.5	61.0	62.1	130.0
	3	100.4	74.4	353.3	380.4	165.3	30.9	134.0	149.0
	4	70.4	204.2	45.0	494.5	115.0	320.0	46.6	75.7
	5	196.9	63.3	41.8	61.3	67.7	218.0	29.6	96.5
	AVG	160.7	100.3	186.2	211.4	119.3	168.2	139.5	99.4
	STDEV	95.6	59.6	158.1	189.2	50.0	106.4	147.1	36.9

Appendix F

Sample overview

The processing parameters of all samples used for the experimental work are found in Table F.0.1.

Table F.0.1: The table gives the vol% of added porosity, which pore former was use and which calcination batch the pellets were made from. The method used to mix the powder and pore former is also included, as well as the use of the pellets.

#	Added porosity	Pore former	Calcination batch	Mixing Procedure	Use
1-12	-	-	0	-	Calcination test
13-19	-	-	1	-	Piezo
20-24	30	CS	1	Wet mixing	Piezo
25-29	10	CS	1	Wet mixing	Broke
30-34	20	CS	1	Wet mixing	Broke
35-39	40	CS	1	Wet mixing	Piezo
40-44	60	CS	2	Wet mixing	Piezo
45-50	50	CS	2	Wet mixing	Piezo
51-56	70	CS	2	Wet mixing	Piezo
57-62	80	CS	2	Wet mixing	Piezo
63-68	10	PMMA	3	Wet mixing	Piezo ¹
69-74	20	PMMA	3	Wet mixing	Piezo
75-80	30	PMMA	3	Wet mixing	Piezo
81-86	40	PMMA	3	Wet mixing	Piezo
87-91	10	CS	4	Wet mixing	Piezo
92-97	20	CS	4	Wet mixing	Piezo
98-103	50	PMMA	4	Dry mixing	Piezo
104-109	60	PMMA	4	Dry mixing	Piezo
110-115	70	PMMA	5	Dry mixing	Piezo
116-121	80	PMMA	5	Dry mixing	Piezo
122-123	-	-	5	-	Broke
124-125	20	PMMA	5	Dry mixing	Hardness
126-127	40	PMMA	5	Dry mixing	Hardness
128-129	60	PMMA	5	Dry mixing	Hardness
130-131	-	-	6	-	Hardness
132-133	20	CS	6	Wet mixing	Hardness
134-135	40	CS	6	Wet mixing	Hardness
136-137	60	CS	6	Wet mixing	Hardness
138-139	80	CS	6	Wet mixing	Broke

¹ Changed BaCO₃ precursor powder was changed from powder with purity >99% to 99.98%. This powder was used for the remaining batches.

References

1. Fedje, K. *Study of Electric Poling Behaviour of Porous Barium Titanate Ceramics* (2016).
2. Mahyudin, F., Widhiyanto, L. & Hermawan, H. Biomaterials and Medical Devices. **58**, 161–181 (2016).
3. Jones, J. R., Ehrenfried, L. M. & Hench, L. L. Optimising bioactive glass scaffolds for bone tissue engineering. *Biomaterials* **27**, 964–973 (2006).
4. Rajabi, A. H., Jaffe, M. & Arinzeh, T. L. Piezoelectric materials for tissue regeneration: A review. *Acta Biomaterialia* **24**, 12–23 (2015).
5. Poinern, G. E. J. *et al.* The synthesis, characterisation and in vivo study of a bioceramic for potential tissue regeneration applications. *Scientific Reports* **4**, 6235 (2014).
6. Jianqing, F., Huipin, Y. & Xingdong, Z. Promotion of osteogenesis by a piezoelectric biological ceramic. *Biomaterials* **18**, 1531–1534 (1997).
7. Baino, F., Novajra, G. & Vitale-Brovarone, C. Bioceramics and Scaffolds: A Winning Combination for Tissue Engineering. *Frontiers in bioengineering and biotechnology* **3**, 202 (2015).
8. Cao, W. & Hench, L. L. Bioactive materials. *Ceramics International* **22**, 493–507 (1996).
9. Giannitelli, S. M., Mozetic, P., Trombetta, M. & Rainer, A. Combined additive manufacturing approaches in tissue engineering. *Acta Biomaterialia* **24**, 1–11 (2015).

10. Zhang, H., Li, J.-F. & Zhang, B.-P. Microstructure and electrical properties of porous PZT ceramics derived from different pore-forming agents. *Acta Materialia* **55**, 171–181 (2007).
11. Richerson, D. W. *Modern Ceramic Engineering : Properties, Processing, and Use in Design* 3rd (ed Taylor and Francis Group) 211–485 (2006).
12. Hutmacher, D. W. Scaffolds in tissue engineering bone and cartilage. *Biomaterials* **21**, 2529–2543. ISSN: 01429612 (2000).
13. Callister, W. D. & Rethwisch, D. G. *Materials Science and Engineering* 8th, 174–179 (Wiley, 2011).
14. Tilley, R. J. D. *Understanding Solids* 2nd (Wiley, 2013).
15. Butscher, A., Bohner, M., Hofmann, S., Gauckler, L. & Müller, R. Structural and material approaches to bone tissue engineering in powder-based three-dimensional printing. *Acta Biomaterialia* **7**, 907–920 (2011).
16. Li, Y. W. & Li, F. X. Large anisotropy of fracture toughness in mechanically poled/depoled ferroelectric ceramics. *Scripta Materialia* **62**, 313–316 (2010).
17. Zhang, P., Li, S. X. & Zhang, Z. F. General relationship between strength and hardness. *Materials Science and Engineering A* **529**, 62–73. ISSN: 09215093 (2011).
18. Yan, J., Clifton, K. B., Mecholsky, J. J. & Reep, R. L. Fracture toughness of manatee rib and bovine femur using a chevron-notched beam test. *Journal of Biomechanics* **39**, 1066–1074 (2006).
19. Mahyudin, F., Widhiyanto, L. & Hermawan, H. Biomaterials in orthopaedics. *Advanced Structured Materials* **58**, 161–181 (2016).
20. Zysset, P. K., Edward Guo, X., Edward Hoffler, C., Moore, K. E. & Goldstein, S. A. Elastic modulus and hardness of cortical and trabecular bone lamellae measured by nanoindentation in the human femur. *Journal of Biomechanics* **32**, 1005–1012 (1999).
21. Park, J. & Lakes, R. S. *Biomaterials - An Introduction* (Springer, 1992).

22. Baxter, F. R., Bowen, C. R., Turner, I. G. & Dent, A. C. E. Electrically active bioceramics: A review of interfacial responses. *Annals of Biomedical Engineering* **38**, 2079–2092 (2010).
23. Jaffe, B. *Piezoelectric ceramics* 1–92 (R. A. N. Publishers, 1971).
24. West, A. *Solid State Chemistry and its Applications* 2nd, 430–445 (Wiley, 2014).
25. Ehmke, M. C., Glaum, J., Hoffman, M., Blendell, J. E. & Bowman, K. J. The effect of electric poling on the performance of lead-free $(1-x)\text{Ba}(\text{Zr}_{0.2}\text{Ti}_{0.8})\text{O}_{3-x}(\text{Ba}_{0.7}\text{Ca}_{0.3})\text{TiO}_3$ piezoceramics. *Journal of the American Ceramic Society* **96**, 3805–3811 (2013).
26. Jin, L., Li, F. & Zhang, S. Decoding the fingerprint of ferroelectric loops: Comprehension of the material properties and structures. *Journal of the American Ceramic Society* **97**, 1–27 (2014).
27. Ahn, A. C. & Grodzinsky, A. J. Relevance of collagen piezoelectricity to "Wolff's Law": A critical review. *Medical Engineering and Physics* **31**, 733–741 (2009).
28. Minary-Jolandan, M. & Yu, M.-F. Nanoscale characterization of isolated individual type I collagen fibrils: polarization and piezoelectricity. *Nanotechnology* **20**, 085706 (2009).
29. Fukada, E. & Yasuda, I. Piezoelectric Effects in Collagen. *Japanese Journal of Applied Physics* **3**, 502B–502B. ISSN: 0021-4922 (1964).
30. HarborMedTech. *HarbourMedTech* <<http://www.harbormedtech.com/bridge>>.
31. Lang, S. B. *et al.* Ferroelectric Polarization in Nanocrystalline Hydroxyapatite Thin Films on Silicon. *Scientific Reports* **3**, 1–6 (2013).
32. Park, J. B. *et al.* Piezoelectric ceramic implants: In vivo results. *Journal of Biomedical Materials Research* **15**, 103–110 (1981).
33. Park, J. B. *et al.* Piezoelectric ceramic implants: A feasibility study. *Journal of Biomedical Materials Research* **14**, 269–277 (1980).

34. Faure, R. *et al.* Alumina foam catalyst supports for industrial steam reforming processes. *Journal of the European Ceramic Society* **31**, 303–312 (2011).
35. Studart, A. R., Gonzenbach, U. T., Tervoort, E. & Gauckler, L. J. Processing routes to macroporous ceramics: A review. *Journal of the American Ceramic Society* **89**, 1771–1789 (2006).
36. De Jonghe, L. C. & Rahaman, M. N. *Sintering of Ceramics* 2003.
37. Roncari, E., Galassi, C., Craciun, F., Capiani, C. & Piancastelli, A. A microstructural study of porous piezoelectric ceramics obtained by different methods. *Journal of the European Ceramic Society* **21**, 409–417 (2001).
38. Wang, Q. *et al.* Effects of pore shape and porosity on the properties of porous LNKN ceramics as bone substitute. *Materials Chemistry and Physics* **109**, 488–491 (2008).
39. Zeng, T., Dong, X. L., Mao, C. L., Zhou, Z. Y. & Yang, H. Effects of pore shape and porosity on the properties of porous PZT 95/5 ceramics. *Journal of the European Ceramic Society* **27**, 2025–2029 (2007).
40. Zeng, T., Dong, X., Chen, S. & Yang, H. Processing and piezoelectric properties of porous PZT ceramics. *Ceramics International* **33**, 395–399 (2007).
41. Yu, S.-W., Kuo, S.-T., Tuan, W.-H., Tsai, Y.-Y. & Su, C.-H. *Ion release from three lead-free piezoelectric ceramics and their physical and cytotoxicity characteristics* 2011.
42. Cook, R. F., Lawn, B. R. & Fairbanks, C. J. Microstructure- Strength Properties in Ceramics: I, Effect of Crack Size on Toughness. *Journal of the American Ceramic Society* **68**, 604–615 (1985).
43. Jiansirisomboon, S. & Watcharapasorn, A. Effects of alumina nano-particulates addition on mechanical and electrical properties of barium titanate ceramics. *Current Applied Physics* **8**, 48–52 (2008).
44. Panteny, S., Bowen, C. R. & Stevens, R. Characterisation of barium titanate-silver composites, part I: Microstructure and mechanical properties. *Journal of Materials Science* **41**, 3837–3843 (2006).

45. Burfoot, J. C. & Taylor, G. W. *Polar Dielectrics and Their Application* 166 (1979).
46. Ball, J. P., Mound, B. A., Nino, J. C. & Allen, J. B. Biocompatible evaluation of barium titanate foamed ceramic structures for orthopedic applications. *Journal of Biomedical Materials Research - Part A* **102**, 2089–2095 (2014).
47. Park, J. B., Kenner, G. H., Brown, S. D. & Scott, J. K. Mechanical property changes of barium titanate (ceramic) after in vivo and in vitro aging. **5**, 267–276 (1977).
48. Roscow, J. I., Lewis, R. W. C., Taylor, J. & Bowen, C. R. Modelling and fabrication of porous sandwich layer barium titanate with improved piezoelectric energy harvesting figures of merit. *Acta Materialia* **128**, 207–217 (2017).
49. Roscow, J., Zhang, Y., Taylor, J. & Bowen, C. R. Porous ferroelectrics for energy harvesting applications. *European Physical Journal: Special Topics* **224**, 2949–2966 (2015).
50. Zhang, Y., Chen, L., Zeng, J., Zhou, K. & Zhang, D. Aligned porous barium titanate/hydroxyapatite composites with high piezoelectric coefficients for bone tissue engineering. *Materials Science and Engineering: C* **39**, 143–149 (2014).
51. Balke, N., Lupascu, D. C., Granzow, T. & Rödel, J. Fatigue of lead zirconate titanate ceramics. I: Unipolar and DC loading. *Journal of the American Ceramic Society* **90**, 1081–1087 (2007).
52. Acros Organics. *Safety data sheet - Poly(methyl methacrylate)* <http://www.acros.com/DesktopModules/Acros_Search_Results/Acros_Search_Results.aspx?search_type=CAS&SearchString=9011147>.
53. Wucherer, L., Nino, J. C. & Subhash, G. Mechanical properties of BaTiO₃ open-porosity foams. *Journal of the European Ceramic Society* **29**, 1987–1993. ISSN: 09552219 (2009).